

# Electroosmotic flow of a rheological fluid in non-uniform micro-vessels

S. Maiti<sup>1,2</sup> \*; S. K. Pandey<sup>1</sup> †; J. C. Misra<sup>3</sup> ‡

<sup>1</sup>*Department of Mathematical Sciences*

*Indian Institute of Technology (BHU),*

Varanasi-221005, India

<sup>2</sup> Department of Mathematics, The LNM Institute of Information Technology  
Jaipur 302031, India

<sup>3</sup> Honorary Visiting Professor, Department of Mathematics,  
Ramakrishna Mission Vidyamandira, Belur Math-711202, Howrah, India

## Abstract

The paper deals with a theoretical study of electrokinetic flow of a rheological Herschel-Bulkley fluid through a cylindrical tube of variable cross-section. The concern of this study is to analyze combined pressure-driven and electroosmotic flow of Herschel-Bulkley fluid. The wall potential is considered to vary slowly and periodically along the axis of the tube. With reference to flow in the micro-vessels, the problem has been solved using the lubrication theory. The Helmholtz-Smoluchowski (HS) slip boundary condition has been employed in this study. Volumetric flow rate  $Q$  is found to be significantly affected by the yield stress parameter  $\nu$  only if an applied pressure force is active. The linear superposition of flow components separately due to the hydrodynamic and electric force occurs only for a strictly uniform tube. This linear relationship fails if non-uniformity appears in either tube radius or in distribution of the electrokinetic slip boundary condition. Moreover, converging/diverging nature of the mean tube radius plays a crucial role on the fluid transport. For the benefit of readers, along with the original contribution, some applications of external electrical stimulation (ES) in the human body and HS slip velocity, studied in the

---

\*Email address: *Corresponding author, maiti000000somnath@gmail.com/somnath.maiti@lnmiit.ac.in (S. Maiti)*

†Email address: *skpandey.apm@itbhu.ac.in (S. K. Pandey)*

‡Email address: *misrajc@gmail.com (J. C. Misra)*

past by previous researchers have been discussed in the paper.

*Keywords: Electroosmotic Flow, Non-Newtonian Fluid, Depletion Layer, Helmholtz-Smoluchowski Slip.*

## 1 Introduction

Movement of fluid in a micro-vessel can take place under the action of electrokinetic forces, or a pressure gradient, or a combination of both of them. Such a flow is called an electroosmotic flow (EOF). The flow takes place due to the interaction of an electric field and mobile ions in the electric double layer (EDL) formed on a charged surface. EDL consists of an inner Stern layer and an outer diffuse layer. The former one is formed at the position where counterions are firmly attached to the surface. The latter one is at the location where counterions outnumber co-ions and form a charged atmosphere shielding the bulk solution from the charged surface [1]. There are several advantages of EOF over pressure-driven flow. The advantages include a more precise flow control, a velocity profile which is much flatter, and flow rate which is less dependent on the vessel-size.

There has been a growing interest in the studies of electroosmotic flow in micro-vessels among engineers and scientists in the emerging areas of micro-fluidics and bio-chips. The mechanism of this flow can be used in various microfluidic applications including miniaturized flow injection analysis [2, 3], and DNA amplification, medical diagnostics, chemical analysis, material synthesis, energy harvesting, clean up, separation, and detection [4, 5].

As mentioned in scientific literatures [6], the first discovery of the electrokinetic effects was made by Reuss [7, 8, 9] by performing experimental investigations on porous clay and it was followed by experiments of Wiedemann [10]. Relating the electric and flow parameters for electrokinetic transport, Helmholtz [11] produced the electric double layer (EDL) theory in 1879. M. von Smoluchowski [12] derived a slip velocity condition for electroosmotically driven flows when EDL thickness was much smaller than the channel dimensions. In order to resolve the velocity field within the EDL, it is essential to place many grid points massively clustered near the wall which create difficulties in the numerical solution of electroosmotic flows. The HS velocity is adopted as a well-known practical alternative to alleviate the above mentioned difficulties [20]. It is an artificial slip velocity imposed at the solid surface in order to incorporate the electroosmotic force in capillaries. For Newtonian fluids, the HS slip velocity is well documented as well as widely adopted by researchers working in this area [24].

The micro-channels, used on a chip for many laboratory applications, have a typical height of 1-100  $\mu m$  and the electroosmotic forces are concentrated within the EDL having an effective thickness in the order of 1-100  $nm$  [6]. Since for electroosmotically driven micro-flows, it is a great challenge in numerical simulation due to this 2-5 orders of magnitude difference in the EDL and the channel length scales; it is required to build up a unified slip condition incorporating the EDL effects by specifying an appropriate velocity-slip condition on the wall [6]. It is generally accepted that task of resolving the double layers is directly computationally impractical [26, 27] for channel widths of the order of tens of microns, since the EDL thickness is then at least two orders of magnitude smaller than the size of the computational domain itself [16]. In fact the order of magnitude is less than about 100  $nm$ .

The HS slip velocity boundary condition is generally used in computational models of flows through micro-channels, because it offers the advantage to approximate the motion of the EDL without resolving the charge density profiles close to the walls [19]. Owing to this, the time of computation is drastically reduced and so the flow equation can be easily solved. Of course, in the region where the wall curvature is sufficiently high, the magnitude of nonphysical velocity is quite large. Keeping in mind that the hydraulic radius varies between 10  $\mu m$  and 100  $\mu m$ , the thickness of the EDL is must less than that of channel, in the case of microfluidic devices. Thus the non-dimensional electrokinetic radius is considerably large. Because of this, the problem of determining the electrical double-layer potential through the use of numerical method turns out to be highly ill-conditioned, whereby determination of different physical quantities becomes very difficult [25]. In order to avoid the calculation of electrical double-layer, an electroosmotic slip condition is generally taken as an alternative to simplify the direct current (DC) electroosmotic flow field [28, 29, 30, 31, 32]. Some authors have used the slip condition in different studies of AC electroosmosis [33, 34, 35].

As hypothesized by Ermakov et al. [3, 13], one can represent the effect of the double layer by substituting the no-slip condition at the channel walls with the velocity outside the double layer in the classical one-dimensional electroosmotic flow solution (e.g. Hunter [14, 15]) in order to reduce the computational time substantially. As examined by Dutta and Beskok [6], the bulk velocity field extended up to the wall had a constant slip value equivalent to Helmholtz-Smoluchowski (HS) slip-velocity. The authors reported that the appropriate slip velocity on the wall was the HS velocity even for finite EDL thickness conditions. It is usually considered in the case of simple micro-channel flows, the EDL at walls is thin enough for “slip velocity” boundary conditions to be employed with sufficient accuracy [16]. MacInnes [17] used the

limits of this approach theoretically in cases characterized by non-uniform liquid properties and complex channel geometries considering the chemically reacting flow through any channel of arbitrary geometrical configuration. The flow is supposed to be produced by electric potential and pressure differences with heat transfer and electrophoresis [16].

For channel widths in the range from several microns to hundreds of microns, MacInnes [17] reported that in the case of local one-dimensional solutions to the Poisson-Boltzmann equation, using appropriate boundary conditions on the walls the expressions for the double layer agree with those obtained by previous researchers. Instead of resolving the EDL directly, it can be replaced by a slip boundary condition for velocity which gives equivalent boundary conditions for the core flow [13, 17, 18]. With consideration of a Debye length of less than 10 *nm* and channel widths of the order of 100  $\mu m$ , they [18] reported that the layer model approximation was excellent for the flow regimes considered in [17].

Some conditions for the validation of the approximation [17] are that (a) the magnitude of the applied electric field  $E = |\mathbf{E}|$  is small compared to the product of the electrostatic field in the EDL ( $\psi_0/\delta$ ) and the ratio of the channel to EDL length scales ( $L/\delta$ ) i.e.  $E \ll (\psi_0/\delta)(L/\delta)$  although the condition is spoiled when the non-dimensional electric field strength rises beyond about ten times its value in a straight channel [17, 19] and (b)  $\kappa^2 L_0^2 \gg \max[1, (E_0 L_0/\zeta_0)^2]$  if  $L_0$  be the channel width,  $E_0$  the electric field strength,  $\zeta_0$  the wall zeta potential and  $\kappa$  the inverse of the Debye length, which represents the characteristic thickness of the double layer [17, 18].

In cases where the double layer thickness is much smaller than the channel size, it is well known [16, 20] that the developed flow in a channel may be reckoned using the HS “slip velocity” boundary condition. This equivalent boundary condition approach is used in the determination of various steady and switching flows in two-dimensional micro-channel junctions [3, 13, 16]. The electroosmotic potential, in the limit of small yet finite Debye layers, loses strength very fast within the thin EDL and a uniform “plug like” velocity profile can be observed in most of the channel [6]. The plug flow behavior has been found in various experiments [21, 22, 23]. The fluid in a capillary travels like plug flow under the action of electroosmotic force as the velocity at the solid surface can be considered to be nonslip and the driving force for fluid movement is acting only within the thin electric double layer. At the limit of very thin double layer, the velocity slips at the wall and it changes from a uniform finite velocity to zero discontinuously at the wall. The velocity deteriorates continuously across the layer and becomes zero at the wall for an actual finite-thickness EDL [24].

Projecting a non-dimensional time scale  $\bar{\omega}$ , the ratio of the diffusion time of momentum

across the electric double-layer thickness to the period of the applied electric field in typical microfluidic applications, Xuan and Li [25] analytically demonstrated that the HS electroosmotic velocity is an appropriate slip condition for alternating current (AC) electroosmotic flows. In the range of applied frequency  $0 \text{ Hz} < f < 16 \text{ MHz}$ , the slip condition approach is appropriate for AC electroosmotic flows in typical microfluidic applications when  $\bar{\omega} < 0.01$  [25]. Due to the thin EDL in most microfluidic applications, we can get a small  $\bar{\omega}$  ensuring that the HS electroosmotic velocity is an appropriate slip condition [25].

However, neglecting the electrical body force in the Cauchy momentum equation and reducing an EOF flow problem to just a boundary condition at surface can reduce the validation of results to limited cases with narrow ranges for physical parameters. Just as an example, in microfluidic problems with small bulk ionic number concentration, this assumption may be not valid anymore. On the other hand, in the pure pressure-driven electrokinetics flow problems (absence of electric force), other physical phenomena such as streaming potential and consequently conduction current are dominant where the employing of the assumption cannot be reasonable.

As considered by Rubin et al. [36], the tangential components on both the boundaries are subject to either Helmholtz-Smoluchowski (HS) slip or Navier slip boundary conditions. HS slip appears over electrically charged surfaces in the presence of an externally applied tangential electric field. Because of the interaction of this field with the excess of net charge in the electric double layer (EDL), the movement of fluid outside the outer edge of the EDL is taking place according to the HS equation [14, 15]. Rubin et al. [36] have assumed a low Dukhin number for their study such that the ionic species concentrations in the bulk and the associated electric field are uniform outside the EDL. Otherwise, non-homogeneity can be introduced into the resultant electric field in the bulk by non-homogeneities of zeta potential and surface conduction [39, 40]. Hydrophobic surfaces may also create slip which is typically modelled by a Navier boundary condition describing that the slip velocity near a flat surface is proportional to the local velocity gradient [36]. Experiments and molecular dynamics simulations over the past few decades have indeed corroborated that slip appears in pressure-driven flows over smooth solvophobic surfaces with slip lengths of the order of nanometres [37, 38].

One may be curious to know how it is possible to apply electric force in the micro-vessel and people normally think that electricity flowing through bodies as an unusual occurrence. As example, they may consider rather unique animals, such as electric eels, or rare events such as being struck by lightning. But, most people cannot realize that electricity is part of everything their body does as from thinking to doing aerobics and even sleeping. Some applications of

electric stimulations that can be applied to a human are discussed below.

Transcranial direct electric stimulation (tDCS) is applied in humans by using direct current over the scalp with the help of electrodes. It was reported that stimulation of cerebellar neurons increased diameter of both adjacent arterioles and the upstream vessels [41, 42]. The reports are also demonstrating the propagation of vascular responses induced by enhanced neural activity [41, 42]. As reviewed by Pulgar [42], tDCS may also modulate blood flow in subcortical structures [43, 44] together with the demonstration of broader effects of tDCS on cerebral blood flow (CBF). As reviewed by Thakral et al. [45], electrical stimulation (ES) therapy enhances venous flow [46, 47, 48, 49] in addition to increased skin perfusion. Transcutaneous electrical nerve stimulation (TENS), consists of a battery-powered device that delivers electrical impulses through electrodes, is performed to evaluate the effect of ES on perfusion.

As mentioned by Rajendran et al. [50], in order to enhance wound healing, the ES is commonly applied by placing electrodes around the wound, which then deliver short bursts of electrical potential having result in electrical currents [51, 52, 53, 54] [in Table 2 [51, 54]]. Watanabe et al. [55] reported that for electrical recording and stimulating, a minimally invasive technique having ability of simultaneously monitoring the activity of a significant number (e.g.,  $10^3$  to  $10^4$ ) of neurons is an absolute prerequisite in developing an effective brain-machine interface. Action potentials can be elicited using a constant current pulse delivered through a bipolar stimulation electrode placed on the spinal cord.

The result, subcontractile ES induces enhanced vascularization in animals, has suggested for one possible route for noninvasive induction of micro-vessels for augmentation of micro-vessel number in patients with peripheral vascular disease [56]. An Elpha 4 Conti transcutaneous electrical stimulator (ERP Group Ltd, Laval, Quebec, Canada) has been applied to deliver localized stimulation at  $10\text{ mA}$ ,  $1.0\text{ V}$  at a frequency of  $8\text{ Hz}$ . Electrodes were used to a  $5\times 5\text{-cm}$  area on the first metatarsal joint of the affected limb and for the 6-week treatment period, stimulation was delivered for three equally spaced one hour periods each day [56].

Action potentials may be generated through cortical neurons by direct electrical stimulation (DES). DES may induce synaptic release of various neurotransmitters that can further react with nearby astrocytes, smooth muscle cells and endothelial cells of the vessel wall [57, 58]. As a result of these reactions, cortical vessels are driven to either vasoconstriction or vasodilatation from the resting state but on the other hand, smooth muscle cells and astrocytes can directly respond to ES [59]: DES of smooth muscle cells may induce vasoconstriction, while DES of astrocytes may drive intracellular calcium waves along the astrocytic syncytium, which

may signal the release of various neuromodulators to direct blood vessels in order to regulate the metabolic supply by changing the local vessel capacity. In addition, ES of brain tissue temporarily enhances extracellular potassium concentration potentially stimulating neural hyperactivity. Enhanced neural activity needs more blood flow, which may activate vasodilatation [57, 60]. Both vasodilatation and vasoconstriction in response to cortical ES can be observed using OR-PAM [58]. For the induction of the preset ES [[58], Figs. 1(b) and 1(c)], a monopolar tungsten electrode (impedance: 1 M $\Omega$ ; tip diameter: 10  $\mu$ m; MicroProbes for Life Science, Gaithersburg, Maryland) was applied into the cortex to a depth of 0.1 to 0.2 mm through the opening at about 2 mm lateral to sagittal suture and 2 mm posterior to bregma.

As available in [61], clinical evidence indicates that by enhancing muscle power and function [62, 63] as well as raising peripheral blood flow [64], neuromuscular electrical stimulation (NMES) through transcutaneous or implantable (i.e., portable) electrodes has beneficial effects on recovery from denervation injuries. As observed by Loaiza et al. [65], increases in muscle blood flow (MBF) and mean arterial pressure ( $47 \pm 10\%$  and  $18 \pm 5\%$ ) over the baseline can be produced by applying psilateral ES (5 V, 20 Hz, for 30 s), however there was no significant changes in MBF in the contralateral muscle.

The arteriolar diameter was observed to rise by  $38.9 \pm 5\%$  following ipsilateral ES [65]. A hook electrode can be applied directly around the left saphenous nerve and ES (0.5 ms, 20 Hz, 1, 3 and 5 V for 30 s) can be delivered using an electrical stimulator (SEN-7203, Nihon Kohden) [65]. To improve blood circulation in diabetic peripheral vessels and potentially treat diabetic peripheral neuropathy, a focused ultrasound (FUS) technique was developed by Tan et al. [66] for effective treatment methods for diabetic peripheral neuropathy. The transducer was driven by in all experiments, a function generator (33 521A, Agilent, Santa Clara, California, USA) and a power amplifier (1040 L, Electronics and Innovation, Rochester, New York, USA) drove and two ring silver wires (UL1423 28 AWG B28-1000, AA electronic Test, USA) were used on the middle three digits as stimulating electrodes to apply an ES with a pulse width of 0.1 ms and a supramaximal intensity [66].

Since the Study of Reuss [7], there are numerous investigations on EOF in the literature. However, studies on EOF of non-Newtonian fluids were limited until recent years. Most physiological fluids behave as a non-Newtonian (rheological) fluid. Many bio-fluids such as blood, protein solutions, DNA solutions; polymeric solutions, and colloidal suspensions are complex fluids, which cannot be treated as Newtonian fluids [67, 68, 69, 18, 70, 71, 72, 73]. These fluids are usually investigated by scientists, engineers and industrialists in microfluidic devices. There-

fore, the need for the study of electroosmotic flow of non-Newtonian fluids has been increasing during recent years. These fluids can be classified according to their rheological natures as shear thinning/thickening, viscoelastic, viscoplastic, structuralized fluids etc.

For Newtonian fluids, the relationship between the driving forces and the flow rate is normally linear. This linear relationship and the so-called Onsager relations are not expected to be followed by non-Newtonian fluids due to the nonlinear fluid rheology. However, considering the effects of wall depletion, Berli and Olivares [67] have reported a linear summation of the parts separately due to the hydrodynamic and electric forcings of EOF of a non-Newtonian fluid. It has been further reported that nonlinear effects are limited to the pressure-driven component of the flow and the Onsager reciprocity, which is described as equality of the non-conjugate streaming coefficients, has been satisfied. However, they studied one-dimensional flow in uniform micro-channels only and thus opened up for an unanswered question if such a linear relationship holds for multi-directional flow.

As described in the articles by Barnes [74], Tuinier and Taniguchi [75] etc., the depletion or skimming layer is a thin layer near a solid wall. In this layer, the fluid is depleted of the macro-molecules which constitute the non-Newtonian behavior of the bulk fluid. Thus, the nature of the fluid in this layer is basically Newtonian solvent. Since it is not accessible to the center of the macro-molecules, its thickness can be comparable with the radius of gyration of the macro-molecules. Berli and Olivares [67] calculated the thickness of this layer. It was enough thick that can cover the EDL and hence the layer may confine the electrokinetic driving force to a portion having the fluid of Newtonian nature. The hydrodynamic driving force is the only force functioning on the bulk non-Newtonian fluid. Berli and Olivares pointed out [67] that the streaming conductance depends only on the Newtonian solvent viscosity and it is independent on the non-Newtonian rheology of the bulk fluid. So, if the fluid is fully Newtonian, Onsager reciprocity can be obtained. Even though the inclusion of depletion layer in the studies on EOF of non-Newtonian fluids had been done by many researchers (cf. Berli [68], Bandopadhyay and Chakraborty [69], Zimmerman et al. [18] and Olivares et al. [76]), the possible nonlinear interplay between the hydrodynamic and electric forcings for a non-parallel flow has not been explored in details. Keeping sight into the flow of bio-fluids in micro-systems, Zimmerman et al. [18], Das and Chakraborty [77] formulated theories on non-Newtonian electrokinetic flow and transport of non-Newtonian fluids in micro-channels.

The power-law model explains shear thinning and shear thickening behaviors of a fluid. But in order to describe the viscoplastic behaviors of a fluid, a yield stress should be introduced.



Among the various types of non-Newtonian models, Herschel-Bulkley fluid model [123] is a more general choice for EOF of fluid which require a finite stress, known as yield stress, in order to deform. Because, this model has advantage over others since the corresponding results for fluids represented by Bingham plastic model, power law model and Newtonian fluid model can be derived as different particular cases from those of the Herschel-Bulkley fluid model. Moreover, Herschel-Bulkley fluid model is expected to give more accurate results than many other non-Newtonian models. Although Newtonian and several non-Newtonian models have been taken into consideration for the study of blood circulation, it is realized (Scott-Blair and Spanner [124]) that Herschel-Bulkley model describes the behaviour of blood very closely. The magnitudes of yield stress in different fluids are different. If the stress is smaller in magnitude than the yield stress, material with a yield stress either does not move or is transported like a rigid body. The material flows with a non-linear stress-strain relationship either as a shear-thickening fluid or a shear-thinning fluid when the yield stress is exceeded. Some examples of fluids behaving in this fashion include food products, paints, plastics, slurries, pharmaceutical products gels, drilling fluids etc. [126, 127]. As reported in [125], Herschel-Bulkley fluids can be used to represent a wide range of fluids such as greases, starch pastes, colloidal suspensions, blood etc. The Herschel-Bulkley fluid model can be also used for simulating debris flow ([127, 130, 131]).

As the velocity profiles in the arterioles having a diameter less than  $0.1\text{ mm}$  examined and explained by Iida [128], blood can be treated fairly well by a Casson fluid model as well as by the Herschel-Bulkley model. However, Scott-Blair and Spanner [124]) observed that blood obeys the Casson equation only in a limited range, but not at very high and very low shear rates. Moreover, there is no difference between the Casson fluid model and Herschel-Bulkley fluid model of the experimental data over the range where the Casson model is valid. It has been reported that the Casson fluid model can be applied for moderate shear rates in smaller diameter tubes although the Herschel-Bulkley fluid model can be considered at still lower shear rate flow in very narrow arteries where the yield stress is high [129]. The Herschel-Bulkley fluid model contains one more parameter than the Casson fluid model does which is expected to provide more detailed information about the blood and other material properties by the use of the Herschel-Bulkley model [129].

There are several natural and industrial yield stress fluids. These includes normal blood with 40% hematocrit (which has yield stress  $4\text{ mPa}$ ) [78] and a mineral suspension with 52 wt. % solids (having yield stress 7 to 11  $\text{Pa}$ ) [79]. Bird et al. [80] carried out a detailed review of viscoplastic materials with a yield stress. These models are explaining the movements of many

yield-stress materials such as pastes, slurries, and suspensions which frequently encountered in industrial problems.

After a lack of effective review for  $\sim 30$  years, since the detailed review by Bird et al. [80, 81], there have recently been a number of studies that provide the breadth of the field [82, 83, 84] dealing with useful introductions [85, 86] and the wonderful 100-year Bingham commemorative collection of researches [87, 88, 89, 90, 91, 92, 93] including targeted reviews and finally the nicely written article by de Souza Mendes and Thompson [94]. A concise summary such as the review by Bird et al. [80] also no longer possible since there has been an enormous expansion of the literature.

The basic and fundamental feature of a viscoplastic fluid is the presence of plugs, namely, at the regions where the stress is below the critical threshold and where the fluid travels like a rigid body. Plugs may happen in the interior of the motion or may adhere to the boundary [95]. Viscoplastic fluids are observed relatively frequently in applications within a thin-film/lubrication/Hele-Shaw setting [95]. In lubrication flows, the singularity of the constitutive equation of a visco-plastic fluid may direct to an apparent inconsistency referred to as the lubrication paradox [96] indicating to the existence or non-existence of true unyielded plug regions within the flow [97]. Indeed, the scaling techniques may forecast a plug velocity that varies in the flow direction so that the rigid region is not truly unyielded in classical lubrication [95]. Many strategies have been proposed in recent years to overcome the paradox [98, 99, 96, 100, 104] based on assuming the existence of a pseudo-plug placed between the unyielded and yielded regions in which the corrections up to the first order are taken into account [101]. The transition of yielded/unyielded happens in a tiny neighborhood of the pseudo-yield surface [95]. The paradox can also be overcome by assuming that the unyielded part may undergo small deformations [102, 103, 105].

The asymptotic analysis of thin viscoplastic films, or viscoplastic lubrication theory, are belong to an earlier time during the 1950s and even comes out in classical texts in 1964 by Pinkus and Sternlicht [107]. But, objections to this theory appeared in the 1980s with the observation that lubrication analyses were apparently inconsistent [82]. As reported by Lipscomb and Denn in 1984, the “lubrication paradox” highlighted how the theory predicted plug regions that were apparently below the yield stress although the velocity field there was not fully rigid [97]. This inconsistency motivated many researchers to study regularized viscoplastic constitutive models and explore unphysical distinguished limits. However, such diversions ultimately turn out unnecessary since the paradox can be resolved by recognizing that the lubrication theory is the

leading-order term of an asymptotic expansion [82]. Moreover, an exploration of higher-order terms provides evidence that the problematic plugs are actually slightly above the yield stress, allowing for their deformation [96, 106]. The regions have been designated with a term pseudo-plugs to emphasize their nature and with their borders referred to as fake yield surfaces. Hence, as a result, there is no lubrication paradox [82].

Limited number of studies of EOF of fluids with a yield stress have been carried out by researchers [67, 108, 109, 110]. We have motivated to know how the yield stress will affect an EOF of a rheological fluid in micro-vessels (which remains largely unknown so far). Since the effect of yield-stress varies qualitatively and quantitatively depending on the viscoplastic models, the concern of this study is to explore the decreasing effect due to a yield stress on the velocity of EOF of a Herschel-Bulkley fluid. For this model, analytical expressions have been derived for the velocity which consists of two regions namely sheared region and non-sheared region. Sheared region is the area where the shear stress exceeds yield stress, while for the non-sheared the opposite is true. The position of the interface, known as the yield surface, separating the sheared and unsheared regions, is within the near-wall electric double layer. Thus the uniform velocity, which located in the unsheared region, is dominating the velocity profile. The uniform velocity arises due to a yield stress and has similarity with the classical plug-like velocity of EOF of a fluid without a yield stress. It is important to mention that the dominant velocity (uniform velocity) here arises because of the result of interaction between rheological properties of fluid and electric forcing. Thus it is subject to more controlling factors than the classical plug-like velocity of EOF of non-yield stress fluid.

Again, since the effect of yield-stress strongly sensitive on the electric forcing, another concern of this study is to analyze EOF of a yield-stress fluid for the situation when the zeta-potential can be large or small. Under the consideration of small electric potential, we may get the Debye-Huckel approximation and it is often applied to obtain the Poisson-Boltzmann equation in linear form. However, this model can cope with both the limits of small and large zeta potentials without the Debye-Huckel approximation. Zeta potential is an essential factor in the model since both shear stress distribution and thus the velocity profile throughout the entire tube requires the zeta potential as a boundary condition. Although, EOF of non-Newtonian fluids under a large zeta potential has been carried out by many researchers, e.g., Bharti et al. [111], Zhao and Yang [112, 113], Vasu and De [114], Babaie et al. [115] and Vakili et al. [116]; they have not included yield stress in their studies.

From the various types of non-Newtonian models, the power-law model has been chosen

mostly to study the electrokinetic flow of non-Newtonian fluids analytically or numerically [67, 68, 76, 111, 112, 114, 115, 117, 118, 119, 120]. However, the nonlinear interaction between the hydrodynamic and electric forcings in driving a power-law or more generally a Herschel-Bulkley fluid through a non-uniform vessels has not been taken into account. It may be noted that it is not generally possible to solve the nonlinear rheological problem of non-Newtonian fluid flow analytically. Nevertheless, most of the analytical researchers [67, 77, 118, 121, 122] on EOF of a power-law fluid have considered simple geometries (i.e. flow over a flat surface, or through a uniform parallel-plate or circular channel).

It is aimed to study pressure-driven and electroosmotic flow of a Herschel-Bulkley fluid in a non-uniform micro-vessels. The study deals with the analytical analysis concerning how the hydrodynamic and electric forcings will interact with each other in driving non-parallel flow of a Herschel-Bulkley fluid through a non-uniform vessel. The study has been analyzed with the help of the lubrication theory [132, 133, 134, 28, 135, 136] together with taking into account the near-wall depletion effect. Therefore, the study is valid particularly for the cases where the Reynolds number is small and the ratio between length scales in the radial direction and the axial direction of the vessel is much smaller than unity. The radius of the vessel as well as the wall charge has been considered to change along with the radius of the tube. It is to be investigated whether for non-parallel flow, the superposition of components due to the two forcings does work linearly for a non-Newtonian fluid, even if we consider a Newtonian depletion layer. Following MacInnes et al. [16], Ng and Qi [137]; the EDL is not resolved directly for the electrokinetic transport and the Helmholtz–Smoluchowski (HS) slip boundary condition [18, 137] has been considered here instead.

We have considered the radius of the vessel of the order of  $100\ \mu m$ . It is much larger than the depletion layer thickness ( $100nm$ ) which is bigger than the EDL thickness ( $10nm$ ). The analysis has been simplified focusing on the bulk fluid flow only (without the direct involvement with the depletion layer). Berli and Olivares [67] used this “single fluid” approach in order to study the hydrodynamic and EOF with slip at the wall as a limiting case.

The current investigation can be applied to model the flows of various bio-fluids in far ranging technological implications, which predominantly exhibit power-law/Herschel-Bulkley fluid (e.g. blood, bio-fluids, protein solutions, DNA solutions, colloidal suspensions, solutions of high polymers and suspensions [67, 71, 74, 77, 109, 110, 111, 116, 117, 118, 122, 137, 138, 139, 140, 141, 142, 143]) behavior and the dynamics of which are not addressed properly. The results can also be utilized as a potential platform to build up microfluidic Lab-on-a-chip based devices

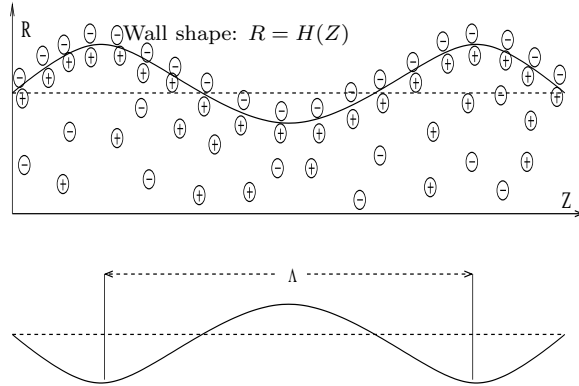


Figure 1: A physical sketch of the electric double layer (EDL) next to a negatively charged solid surface of the problem for transverse pressure-driven and electroosmotic flow of a Herschel-Bulkley fluid through a non-uniform tube with undulated walls and charge-modulated surfaces.

dealing with the power-law/Herschel-Bulkley type bio-fluids, with electrokinetically driven flow actuation mechanisms. Nonlinear effects, which are expected when complex fluids are subjected to electric potential and/or pressure gradients in micro-channels, are vital aspect for the design and operation of microfluidic chips. Thus the interactions between fluid rheology, slip wall velocity, and EDL phenomena may be exploited to achieve a surprising augmentations in the device throughput over characteristic regimes of interest.

## 2 Formulation

Pressure-driven and Electroosmotic flow (EOF) of a non-Newtonian fluid is intended to analyze theoretically in an axisymmetric cylindrical micro-vessel. The fluid is undertaken as an incompressible viscous Herschel-Bulkley fluid under the consideration that the radius and the wall potential may vary slowly and periodically along the axis of the vessel. In addition, the diverging/tapered nature of the mean tube radius has also been incorporated in this study.

Let us assume  $(R, \theta, Z)$  as the cylindrical polar coordinates of the location of any fluid particle (cf. Fig. 1) in the micro-vessel.  $R$  is measured along the radius of the vessel,  $Z$  is being measured along the axis of the vessel and  $\theta$  is considered as the rotational coordinate.  $R = H(Z)$  (cf. Fig. 1) represents the wall of the micro-vessel and the wall potential is taken as  $\xi = \xi(Z)$ . Both  $H(Z)$  and  $\xi(Z)$  have been treated as periodic functions of  $Z$  with the same wave length  $\lambda$ . The radius of the vessel is considered as much smaller than  $\lambda$  so that ratio between them to

be much smaller than unity. In order to apply lubrication theory, the Reynolds number of the flow is considered to be small together with small ratio of the tube radius and wavelength as said above.

The EDL is a very thin region close to the charged surface where an excess of counterions over coions in order to neutralize the surface charge [20]. Thus, a net fluid flow can be driven in the desired direction when imposing external electric field [24]. The application of a time-periodic external electric field creates a net body force on the free ions inducing a time-periodic bulk motion within the electric double layer (EDL) [144]. (governing equation with electrical body force)

The non-Newtonian bulk fluid has been treated as a viscous Herschel-Bulkley fluid. It has been considered that the walls are non-adsorbing indicating that the layer very near the boundary is a depletion layer. In this layer the fluid, owing to the absence of the inclusion of the macromolecules, is much less viscous than the bulk fluid and we may treat it as Newtonian. We further consider that the electric double layer is thinner than the depletion layer. As a result, the electrokinetic effect can be confined to the region of Newtonian fluid near the boundary of the vessel. Moreover, the depletion layer thickness is considered much smaller than the radius of the tube. Thus, the electrokinetic forcing has been simplified to a Helmholtz-Smoluchowski (HS) Electroosmotic slip velocity [18]. As mentioned by Dutta and Beskok [6], the HS electroosmotic velocity can be generated as a result from the balance between the viscous diffusion terms and the electroosmotic forces in the absence of the pressure gradients.

However, the employed simplifying assumption on HS slip velocity can be reasonable in cases with very thin EDL or in flow fields with not strong non-Newtonian rheological behavior. It is important to mention that there are a lot of studies in the literature which provide equations to modify the HS velocity for non-Newtonian fluid flows.

EOF of rheological fluid has been considered to be governed by the Navier-Stokes equations

$$\nabla \cdot \mathbf{V} = 0 \tag{1}$$

$$\text{and } \rho \frac{d\mathbf{V}}{dt} = \nabla \sigma + \rho_e \mathbf{E}. \tag{2}$$

Here  $\mathbf{V}$  represents the velocity vector,  $\mathbf{E}$  is the electrical field strength applied to the micro-vessel,  $\rho$  being the fluid density,  $\rho_e$  is the local net charge density and  $\frac{d}{dt}$  is the material time-derivative.  $\sigma$  defines the Cauchy stress tensor which can be expressed as

$$\sigma = -PI + T,$$

in which

$$T = 2\mu E_{ij} + \eta IS \text{ and } S = \nabla \cdot \mathbf{V},$$

$E_{ij}$  being the symmetric part of the velocity gradient, is defined by

$$E_{ij} = \frac{1}{2}[L + L^T],$$

where  $L = \nabla \mathbf{V}$ .

$-PI$  is known as the indeterminate part of the stress due to the constraint of incompressibility.

We denote  $\mu$  and  $\eta$  as viscosity parameters.

As mentioned above, Herschel-Bulkley model represents the combined effect of Bingham plastic and power-law behavior of the fluid. It is well known that when strain-rate  $\dot{\gamma}$  is less than  $\frac{\tau_0}{\mu_0}$ , the fluid behaves like a viscous fluid with constant viscosity  $\mu_0$ . But as the strain rate increases and the yield stress threshold ( $\tau_0$ ) is reached, the fluid behavior is better described by a power law of the form

$$\tau_{ij} = \begin{cases} (\mu \dot{\gamma}^{n-1} + \frac{\tau_0}{\dot{\gamma}}) \dot{\gamma}_{ij} & : \text{ for } \tau \geq \tau_0, \\ \dot{\gamma}_{ij} = 0 & : \text{ for } \tau < \tau_0 \end{cases}, \quad (3)$$

$$(4)$$

in which

$$\dot{\gamma}_{ij} = \left( \frac{\partial U_i}{\partial X_j} + \frac{\partial U_j}{\partial X_i} \right), \quad \tau = \sqrt{\frac{\tau_{ij} \tau_{ij}}{2}}, \quad \dot{\gamma} = \sqrt{\frac{\dot{\gamma}_{ij} \dot{\gamma}_{ij}}{2}}. \quad (5)$$

Here  $\mu$  and  $n$  denote respectively the consistency factor and the power law index. Where  $n < 1$  and  $n > 1$  correspond to a shear thinning fluid and shear thickening fluid respectively.

Lee et al. [145] reported that the driving force for the electroosmotic flow,  $\rho_e \mathbf{E}$ , appears only in EDL as the local net charge density is non-zero only in the EDL. The EOF velocity varies sharply in a thin layer of liquid near the wall from zero at the channel wall surface to an approximately constant value at the outer edge of the EDL [145].

The general micro-channel height deviates from 10 to 100  $\mu m$  and thickness of EDL changes from 1 to 10  $nm$  in a typical microfluidic device [146]. Buffer solutions have a concentration of the order of  $mM$  for most on-chip microfluidic applications resulting in a very thin EDL [145, 144]. As a example, a solution with a 10  $mM$  concentration has a EDL thickness of approximately 10  $nm$  that is negligible in comparison with the micro-channel diameter (e.g. 100  $\mu m$ ) [145].

Hence, the driving force term  $\rho_e \mathbf{E}$  will be dropped off in the governing equation and the bulk fluid flow, outside of the EDL region, can be modeled by replacing the electroosmotic body

force with help of introduction of a HS slip boundary condition at the channel wall [145, 144]. Moreover, as reported by Kim et al. [146],  $\rho\mathbf{E}$ , can be dropped off and the electroosmotic effect can be replaced by introducing a slip velocity at the channel wall for the modeling purpose of the bulk fluid flow outside the EDL following HS formulation on the basis of the assumption that both viscosity and permittivity are constant and they are independent of time and space [146].

Although the HS formulation is originally introduced for steady state DC EOF, it can be employed for low frequency AC (or time periodic) EOF since the charge relaxation frequency ( $f_c = (1/2\pi)(\sigma/\epsilon) \cong 10^6 \sim 10^8 \text{ Hz}$ ) be much larger for equilibrium distribution of ions in the electrical double layer [147]. Furthermore, HS formulation is widely employed for non-uniform electroosmotic flow model in capillaries [148] and micro-channels [149, 145, 150].

This slip boundary condition can also be used for time-periodic EOF since the applied electric field frequency ( $10^2 \sim 10^5 \text{ Hz}$ ) is less than the charge relaxation frequency ( $10^6 \sim 10^8 \text{ Hz}$ ) [151] although it was originally introduced for steady-state EOF. Furthermore, the Helmholtz-Smoluchowski development-based slip boundary condition is widely employed for non-homogeneous surface charges and time-periodic EOF analysis [146, 145, 148, 150, 132]. Since the Debye length of the electric double layer is less than  $10 \text{ nm}$  in the micro-channels used on a chip for many laboratory applications [18], inside such a thin region it is hardly available any polymer molecules due to the depletion effect [75] indicating that the solvent viscosity to be the appropriate viscosity for determination of the boundary HS slip velocity [18].

Thus replacing the electroosmotic body force (i.e.  $\rho_e\mathbf{E}$ ) with help of introduction of a HS slip boundary condition, the governing equations (Navier-Stokes equations) of the Herschel-Bulkley fluid may be written in the form

$$\rho \left( \frac{\partial U}{\partial t} + U \frac{\partial U}{\partial Z} + V \frac{\partial U}{\partial R} \right) = - \frac{\partial P}{\partial Z} + \frac{1}{R} \frac{\partial(R\tau_{RZ})}{\partial R} + \frac{\partial \tau_{ZZ}}{\partial Z}, \quad (6)$$

$$\rho \left( \frac{\partial V}{\partial t} + U \frac{\partial V}{\partial Z} + V \frac{\partial V}{\partial R} \right) = - \frac{\partial P}{\partial R} + \frac{1}{R} \frac{\partial(R\tau_{RR})}{\partial R} + \frac{\partial \tau_{RZ}}{\partial Z}. \quad (7)$$

The following non-dimensional variables will be introduced in the analysis:

$$\begin{aligned} \bar{Z} &= \frac{Z}{\lambda}, \quad \bar{R} = \frac{R}{a_0}, \quad \bar{U} = \frac{U}{c}, \quad \bar{V} = \frac{V}{c\delta}, \quad \delta = \frac{a_0}{\lambda}, \quad \bar{P} = \frac{a_0^{n+1}P}{\mu c^n \lambda}, \quad \bar{t} = \frac{ct}{\lambda}, \quad h = \frac{H}{a_0}, \quad \phi = \frac{d}{a_0}, \\ Re &= \frac{\rho a_0^n}{\mu c^{n-2}}, \quad \bar{\tau}_0 = \frac{\tau_0}{\mu \left(\frac{c}{a_0}\right)^n}, \quad \bar{\tau}_{RZ} = \frac{\tau_{RZ}}{\mu \left(\frac{c}{a_0}\right)^n}, \quad \bar{\tau}_{ZZ} = \frac{\tau_{ZZ}}{\mu \delta \left(\frac{c}{a_0}\right)^n}, \quad \bar{\tau}_{RR} = \frac{\tau_{RR}}{\mu \delta \left(\frac{c}{a_0}\right)^n}, \end{aligned} \quad (8)$$



where we consider  $\lambda$ ,  $a_0$  as the length scales for velocity variations in the  $x, y$ -direction, respectively and  $c$  as a scale for the velocity in the  $x$ -direction. The equation governing the flow of the fluid can now be rewritten in the form (dropping the bars over the symbols):

$$Re\delta \left( \frac{\partial U}{\partial t} + U \frac{\partial U}{\partial Z} + V \frac{\partial U}{\partial R} \right) = -\frac{\partial P}{\partial Z} + \frac{1}{R} \frac{\partial \left( \Phi \left( R \frac{\partial U}{\partial R} + R \delta^2 \frac{\partial V}{\partial Z} \right) \right)}{\partial R} + 2\delta^2 \frac{\partial \left( \Phi \frac{\partial U}{\partial Z} \right)}{\partial Z}, \quad (9)$$

$$Re\delta^3 \left( \frac{\partial V}{\partial t} + U \frac{\partial V}{\partial Z} + V \frac{\partial V}{\partial R} \right) = -\frac{\partial P}{\partial R} + \delta^2 \frac{2}{R} \frac{\partial \left( R \Phi \frac{\partial V}{\partial R} \right)}{\partial R} + \delta^2 \frac{\partial \left( \Phi \left( \frac{\partial U}{\partial R} + \delta^2 \frac{\partial V}{\partial Z} \right) \right)}{\partial Z} \quad (10)$$

$$\begin{aligned} , \text{ where } \Phi = & \left| \sqrt{2\delta^2 \left\{ \left( \frac{\partial V}{\partial R} \right)^2 + \left( \frac{V}{R} \right)^2 + \left( \frac{\partial U}{\partial Z} \right)^2 \right\} + \left( \frac{\partial U}{\partial R} + \delta^2 \frac{\partial V}{\partial Z} \right)^2} \right|^{n-1} \\ & + \tau_0 \left| \sqrt{2\delta^2 \left\{ \left( \frac{\partial V}{\partial R} \right)^2 + \left( \frac{V}{R} \right)^2 + \left( \frac{\partial U}{\partial Z} \right)^2 \right\} + \left( \frac{\partial U}{\partial R} + \delta^2 \frac{\partial V}{\partial Z} \right)^2} \right|^{-1} \end{aligned} \quad (11)$$

For the case  $\delta \ll 1$  and  $\delta Re \ll 1$  (i.e. the lubrication approximation), the governing equations, describing the flow in terms of the dimensionless variables (8), assume the form

$$0 = -\frac{\partial P}{\partial Z} + \frac{1}{R} \frac{\partial \left( R \frac{\partial U}{\partial R} \left| \frac{\partial U}{\partial R} \right|^{n-1} + R\tau_0 \right)}{\partial R} \quad (12)$$

$$\text{and } 0 = -\frac{\partial P}{\partial R}. \quad (13)$$

The boundary conditions [6, 18, 20, 8, 146, 36, 144] in non-dimensional co-ordinates take the form

$$\frac{\partial U}{\partial R} = 0, \quad \tau_{RZ} = 0 \text{ at } R = 0 \quad \text{and} \quad (14)$$

$$U = U_s(Z) = -\frac{\zeta E_Z}{\mu_s} \xi(Z) \text{ at } R = h(Z), \quad (15)$$

where  $\zeta$  &  $\mu_s$  denote the permittivity and dynamic viscosity of the solvent in the depletion layer respectively and  $E_Z$  is the applied axial electric field.

Applying the condition (14), the solution of equation (12) is found as

$$\frac{\partial U}{\partial R} \left| \frac{\partial U}{\partial R} \right|^{n-1} + \tau_0 = \frac{R}{2} \frac{\partial P}{\partial Z}. \quad (16)$$

Now, using the condition (15), the solution of equation (16) can be expressed as

$$U(R, Z, t) = U_s(Z) + \frac{1}{(m+1)P_1} \left[ (P_1 h - \tau_0)^{m+1} - (P_1 R - \tau_0)^{m+1} \right], \quad 0 \leq R \leq h(Z); \quad (17)$$

where  $P_1 = -\frac{1}{2} \frac{\partial P}{\partial Z}$  and  $m = \frac{1}{n}$ .

If we consider  $\tau_0 = 0$  (i.e. the absence of yeild stress) and  $n = 1$  (i.e. for Newtonian fluid), the equation (17) can be simplified as

$$U(R, Z, t) = U_s(Z) + \frac{P_1}{2} [h^2 - R^2], \quad 0 \leq R \leq h(Z). \quad (18)$$

Thus, the results are found to coincide with those obtained by Dutta and Beskok [6] (Ref. equation (13) and (14) of [6]), when the flow in two-dimensional channel is replaced by the flow in axisymmetric tube. This observation may be considered as a validation of the present study.

The radius of the plug flow region,  $R_0$  is given by

$$\frac{\partial U}{\partial R} = 0 \quad \text{at } R = R_0.$$

Which in view of (17), is obtained as

$$R_0 = \tau_0 / P_1.$$

Considering  $\tau_{RZ} = \tau_h$  at  $R=h$ , we find  $h = \tau_h / P_1$  and

$$\frac{R_0}{h} = \frac{\tau_0}{\tau_h} = \nu \text{ (say)}, \quad 0 < \nu < 1. \quad (19)$$

We have then obtained the expression of the plug velocity as

$$U_P = \frac{(P_1 h - \tau_0)^{m+1}}{(m+1)P_1}. \quad (20)$$

The instantaneous rate of volume flow through the micro-vessel,  $Q$ , may then be given by

$$\begin{aligned} Q &= 2 \int_0^{R_0} RU dR + 2 \int_{R_0}^h RU dR \\ &= U_s(Z)h^2 + \frac{P_1^m (h - R_0)^{m+1} (h^2(m^2 + 3m + 2) + 2R_0 h(m + 2) + 2R_0^2)}{(m+1)(m+2)(m+3)}, \quad m = \frac{1}{n}. \end{aligned} \quad (21)$$

For  $P_1 < 0$  (i.e., under adverse pressure gradient), the stress is positive. From equation (21), it is clear that  $P_1 < 0$  where  $Q < U_s(Z)h^2$  and  $P_1 > 0$  where  $Q > U_s(Z)h^2$ . A single expression for  $P_1$ , the pressure gradient, as a function of the flow rate, is then obtained as

$$\begin{aligned} P_1 &= -\frac{1}{2} \frac{\partial P}{\partial Z} = \left[ \frac{(m+1)(m+2)(m+3)}{(h - R_0)^{m+1} (h^2(m^2 + 3m + 2) + 2R_0 h(m + 2) + 2R_0^2)} \right]^n |Q - U_s(Z)h^2|^{n-1} (Q - U_s(Z)h^2) \\ &= \left[ \frac{(m+1)(m+2)(m+3)}{h^{m+3} (1 - \nu)^{m+1} ((m^2 + 3m + 2) + 2\nu(m+1) + 2\nu^2)} \right]^n |Q - U_s(Z)h^2|^{n-1} (Q - U_s(Z)h^2). \end{aligned}$$

The net pressure drop across one wavelength may now be evaluated as

$$\Delta P = \int_0^1 \left( \frac{\partial P}{\partial Z} \right) dZ . \quad (23)$$

For the Newtonian fluid ( $n = 1$ ), the solution of the equation (23) is given by

$$Q_{n=1} = (\Delta P - I_2)/I_1, \quad (24)$$

where

$$I_1 = -24 \int_0^1 \frac{1}{(h - R_0)^2(3h^2 + 3R_0h + R_0^2)} dZ,$$

$$I_2 = -24 \int_0^1 \frac{U_s(Z)h^2}{(h - R_0)^2(3h^2 + 3R_0h + R_0^2)} dZ.$$

For the uniform vessel, a special case where  $h$  and  $U_s(Z)$  are both constants, equation (23) may also yield

$$Q_{uniform} = \mp \frac{(h - R_0)^{m+1}(h^2(m^2 + 3m + 2) + 2R_0h(m + 2) + 2R_0^2)}{(m + 1)(m + 2)(m + 3)} |\Delta P|^m + U_s(Z)h^2, \quad (25)$$

where the upper or lower signs are for  $\Delta P > 0$  or  $\Delta P < 0$  respectively.

In general, the equation (23) cannot be integrated in closed form. For further investigation of the problem under consideration, it may be solved numerically under an efficient iterative solution scheme. The left side of equation (23) has been calculated based on the  $i$ th trial flow rate  $Q^{(i)}$  in order to get the  $i$ th trial pressure drop  $\Delta P^{(i)}$ . It is then compared with the given  $\Delta P$ . The following equations show how the  $(i + 1)$ th flow rate will be found by the difference of the two:

$$Q^{(i+1)} = Q^{(i)} + \frac{\Delta P - \Delta P^{(i)}}{d\Delta P/dQ}, \quad (26)$$

$$\text{where } \frac{d\Delta P}{dQ} = n \left\{ \frac{(m + 1)(m + 2)(m + 3)}{(m + 1)(m + 2) + 2(m + 1)\nu + 2\nu^2(1 - \nu)^{(k+1)}} \right\}^n \int_0^1 \frac{|Q - U_s(Z)h^2|^{(n-1)}}{h^{(3n+1)}} dZ. \quad (27)$$

We have taken the Newtonian flow rate  $Q_{n=1}$  given by equation (25) as the initial value of  $Q^{(1)}$ . It is normally observed that the solution converges in 5 iterations. However, the accuracy of the solution depends on the numerical evaluation of the definite integrals and time required for these solutions is much more when the tube radius is of converging/diverging nature.

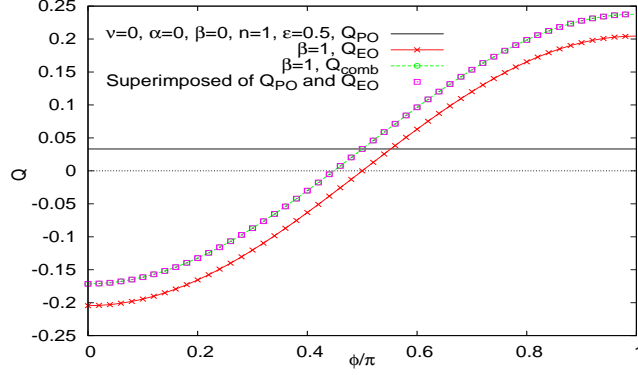


Figure 2: Variation of flow rate  $Q$  with the phase shift  $\phi$  when  $k = 0$ ;  $\Delta P = 0, -1$ ;  $\nu = 0$ ;  $\epsilon = 0.5$ ;  $\alpha = 0$ ;  $\beta = 0, 1$  for a Newtonian fluid.

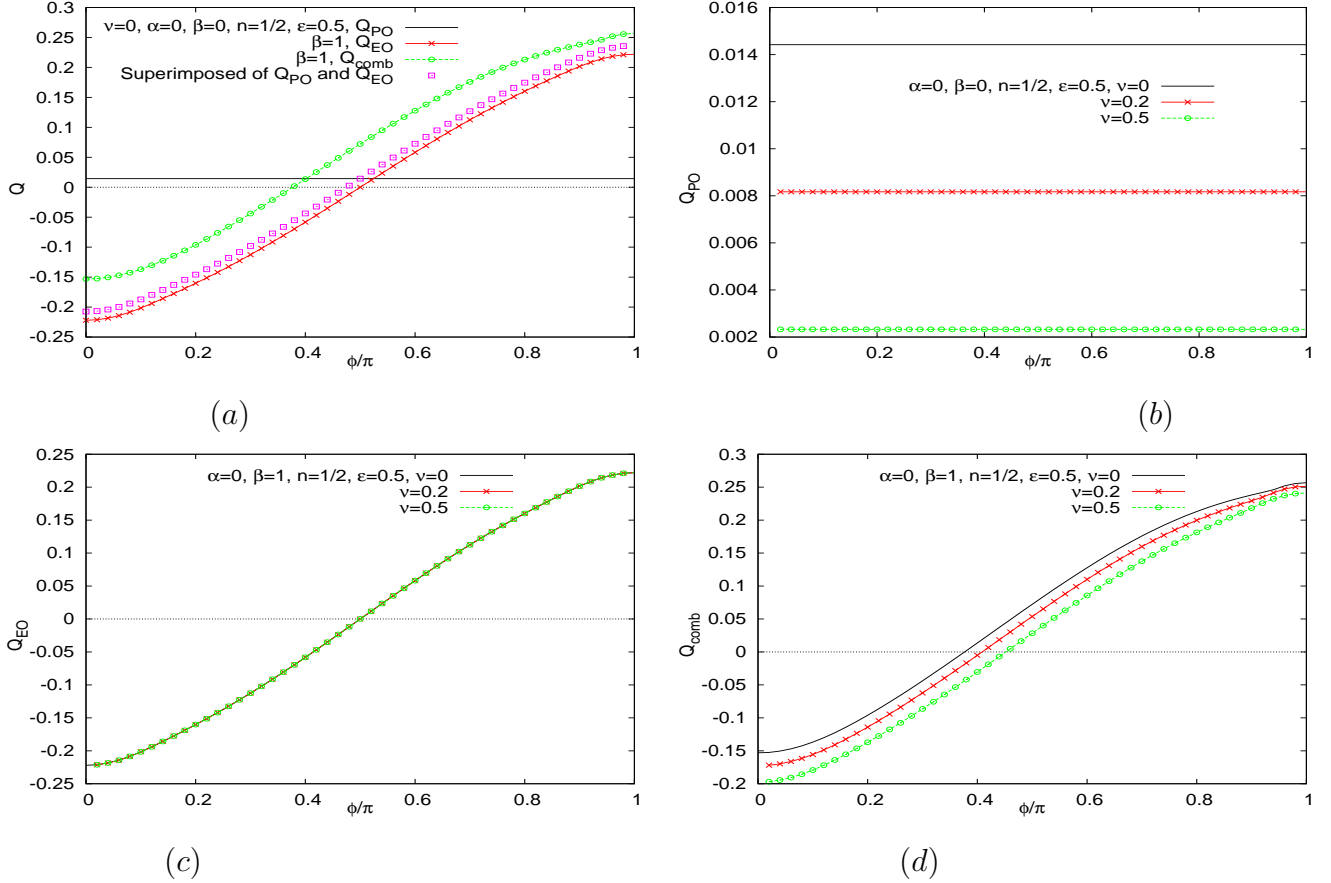


Figure 3: Variation of flow rate  $Q$  with the phase shift  $\phi$  when  $k = 0$ ;  $\Delta P = 0, -1$ ;  $\nu = 0$  to  $0.5$ ;  $\epsilon = 0.5$ ;  $\alpha = 0$ ;  $\beta = 0, 1$  for a shear-thinning fluid.

### 3 Quantitative Investigation

In this section, our aim is to study the problem and present the computational results for the said quantities graphically. Computations of the quantities have been carried out by extensive use of the software Mathematica. In order to get the computational results, 8 input, i.e.  $n$ ,  $\Delta P$ ,  $\epsilon$ ,  $\alpha$ ,  $\beta$ ,  $\phi$ ,  $k$  and  $\nu$  have been used. As long as  $h$  and  $U_s$  are considered as slowly varying functions of  $Z$ , equations (17), (22)-(25) are valid for them. The radius of the tube and HS slip velocity have been treated as the following sinusoidal functions

$$h = 1 + kZ + \epsilon \cos(2\pi Z), \quad U_s = \alpha + \beta \cos(2\pi Z + \phi); \quad (28)$$

where  $\alpha$  stands for the mean HS slip velocity,  $\epsilon$  being the amplitudes of the wall shape,  $\beta$  for slip modulation and  $\phi$  for the phase shift between the two modulation waves. Here,  $k$  is a constant parameter whose positive value means that the mean tube radius is of diverging nature, while the negative value of it indicates the tapered nature of the mean tube radius. The above idealized wave forms of the geometric and electrokinetic modulation may provide indicative results for the physics involved in this problem.

It is easy to note that, in either of the two particular cases, e.g. Newtonian limit or uniform tube radius, there is no essential coupling between the two forces hydrodynamic and electrokinetic. Hence the flow is a linear combination of the hydrodynamic and electrokinetic effects in these cases. For another special case where  $\Delta P = 0$  and walls are flat ( $\epsilon = 0$ ), it is worthwhile to note that

$$Q = \alpha \text{ for any } n \text{ and } \beta. \quad (29)$$

In the numerical discussion, these limiting and special cases will be further discussed.

In order to inspect the issue of linear superposition of the hydrodynamic and electrokinetic effects closely, we define the following types of flow rate  $Q$ :

$$Q_{PO} = \text{rate of flow due to hydrodynamic forcing } \Delta P \text{ only}, \quad (30)$$

$$Q_{EO} = \text{rate of flow due to electric forcing } U_s \text{ only}, \quad (31)$$

$$Q_{comb} = \text{rate of flow due to combined action of } \Delta P \text{ and } U_s. \quad (32)$$

For different values of the phase shift  $\phi$  (between the two modulation waves),  $n$  (flow index number),  $\nu$ ,  $\alpha$ ,  $\beta$ ,  $\epsilon$ , Figs. 2-11 present the distribution of flow rate  $Q$  for the cases of  $Q_{PO}$ ,  $Q_{EO}$  and  $Q_{comb}$ . Figs. 2-4 show the the variation of flow rates with the phase  $\phi$  for the cases

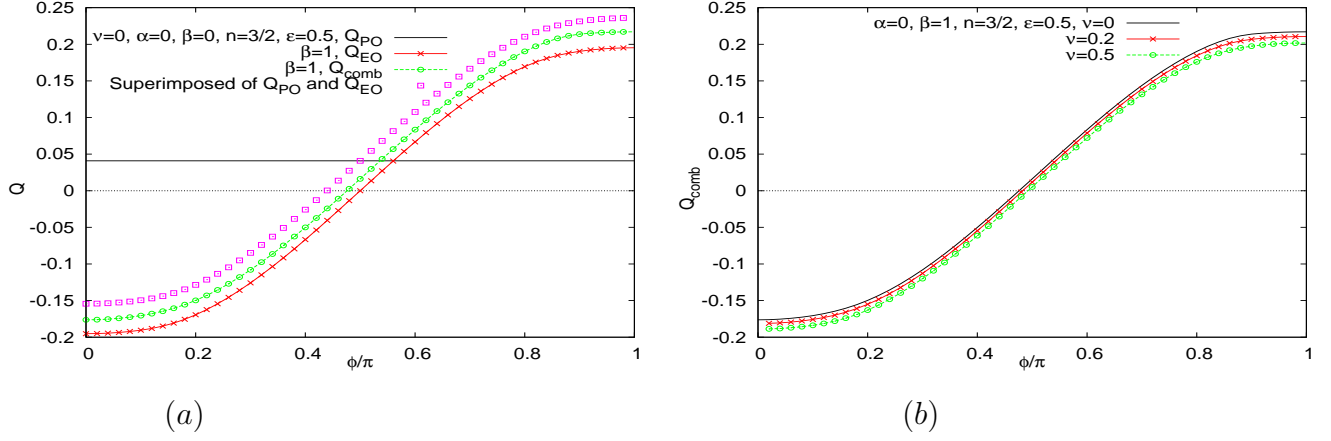


Figure 4: Variation of flow rate  $Q$  with the phase shift  $\phi$  when  $k = 0$ ;  $\Delta P = 0, -1$ ;  $\nu = 0$  to  $0.5$ ;  $\epsilon = 0.5$ ;  $\alpha = 0$ ;  $\beta = 0, 1$  for a shear-thickening fluid.

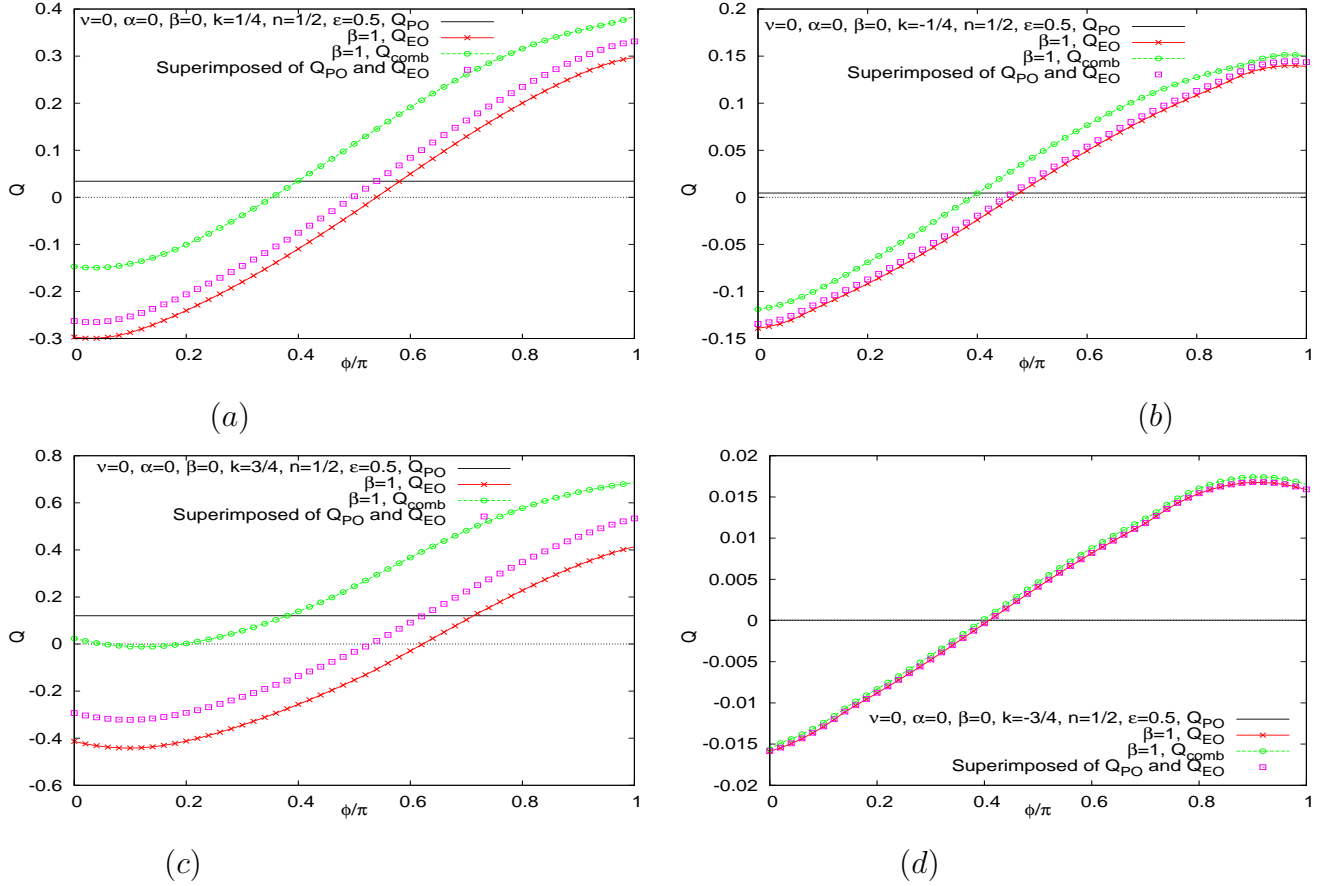


Figure 5: Variation of flow rate  $Q$  with the phase shift  $\phi$  when  $\Delta P = 0, -1$ ;  $\nu = 0$ ;  $\epsilon = 0.5$ ;  $\alpha = 0$ ;  $\beta = 0, 1$  for a shear-thinning fluid in tube (with mean radius is of diverging/tapered nature).

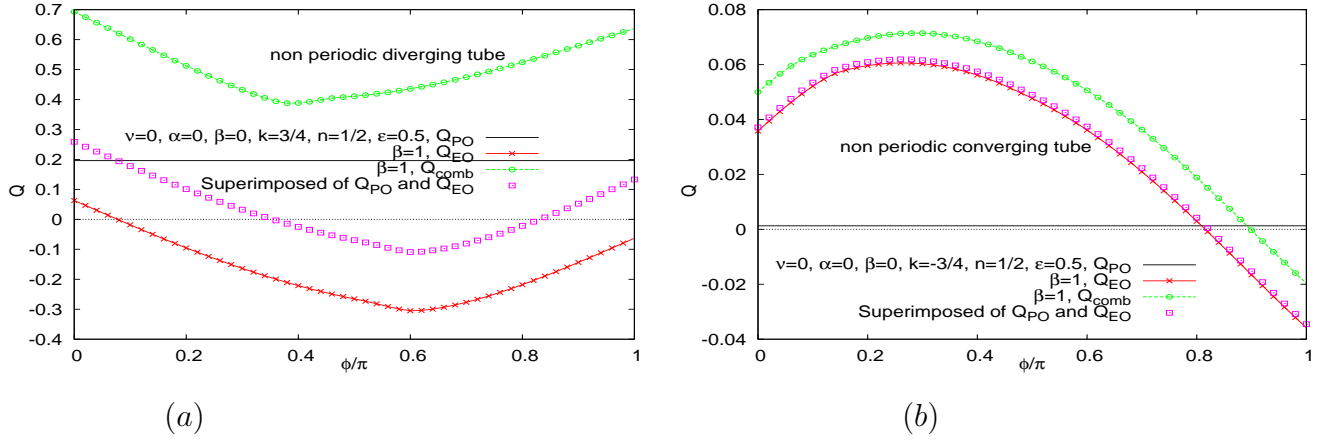


Figure 6: Variation of flow rate  $Q$  with the phase shift  $\phi$  when  $\Delta P = 0, -1$ ;  $\nu = 0$ ;  $\epsilon = 0.5$ ;  $\alpha = 0$ ;  $\beta = 0, 1$  for a shear-thinning fluid in a diverging/tapered tube.

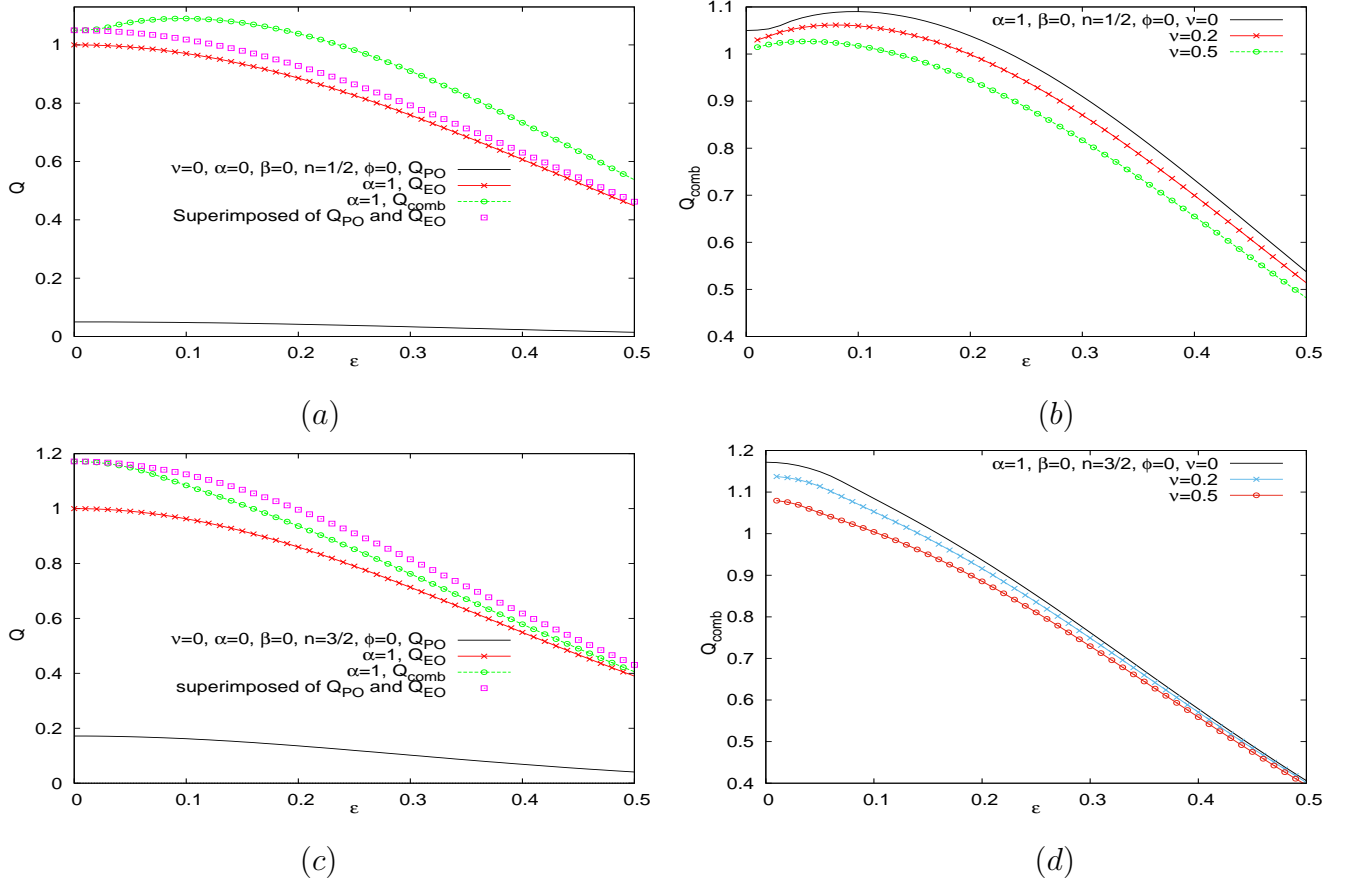


Figure 7: Variation of flow rate  $Q$  with the wall undulation amplitude  $\epsilon$  when  $k = 0$ ;  $\Delta P = 0, -1$ ;  $\nu = 0$  to  $0.5$ ;  $\phi = 0$ ;  $\alpha = 0, 1$ ;  $\beta = 0$  for a shear-thinning and a shear-thickening fluid.

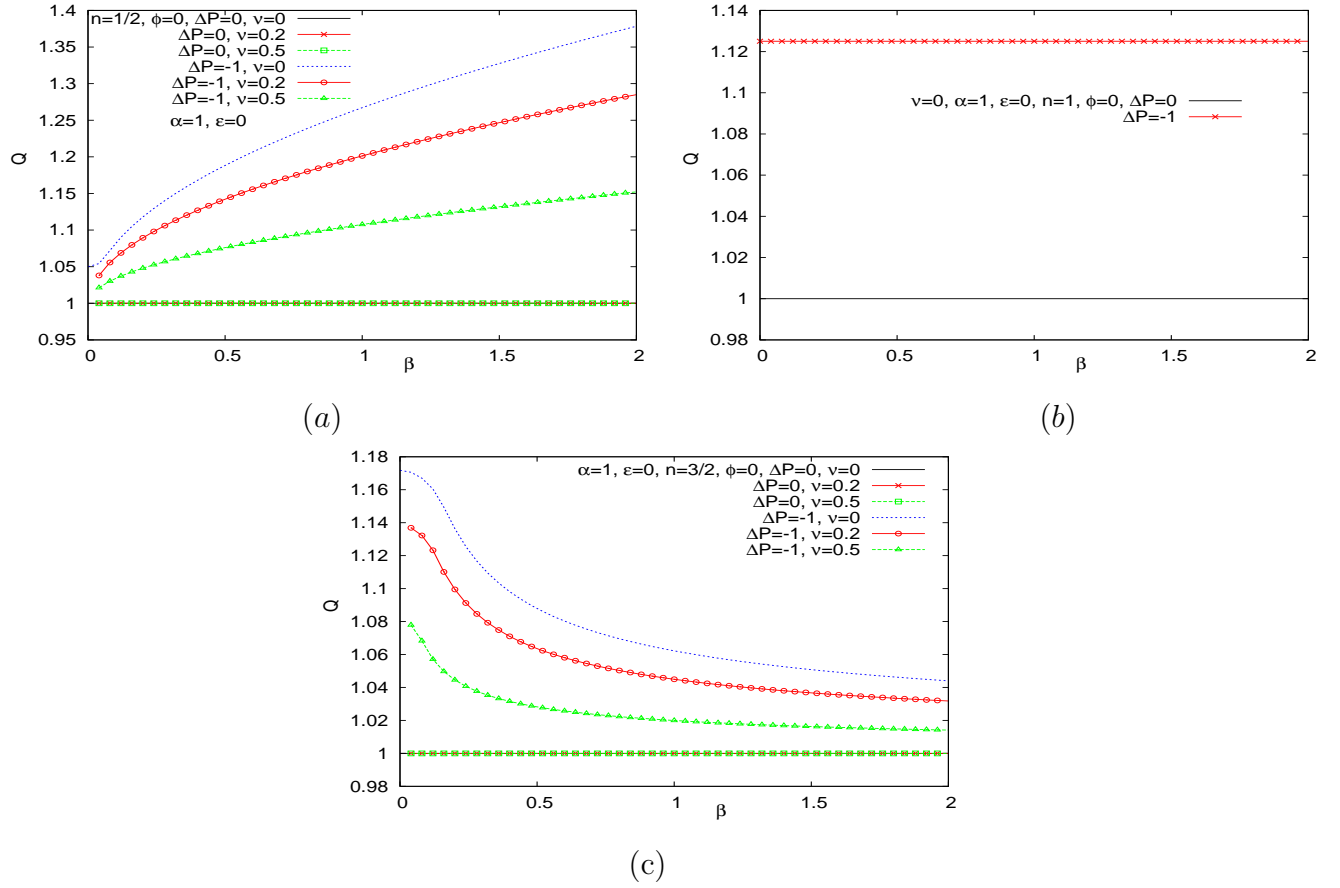


Figure 8: Variation of flow rate  $Q$  with the HS slip modulation amplitude  $\beta$  for  $k = 0$ ;  $\Delta P = 0, -1$ ;  $\nu = 0$  to  $0.5$ ;  $\phi = 0$ ;  $\alpha = 1$ ;  $\epsilon = 0$  (a) Newtonian fluid, (b) Shear-thinning fluid (c) Shear-thickening fluid.



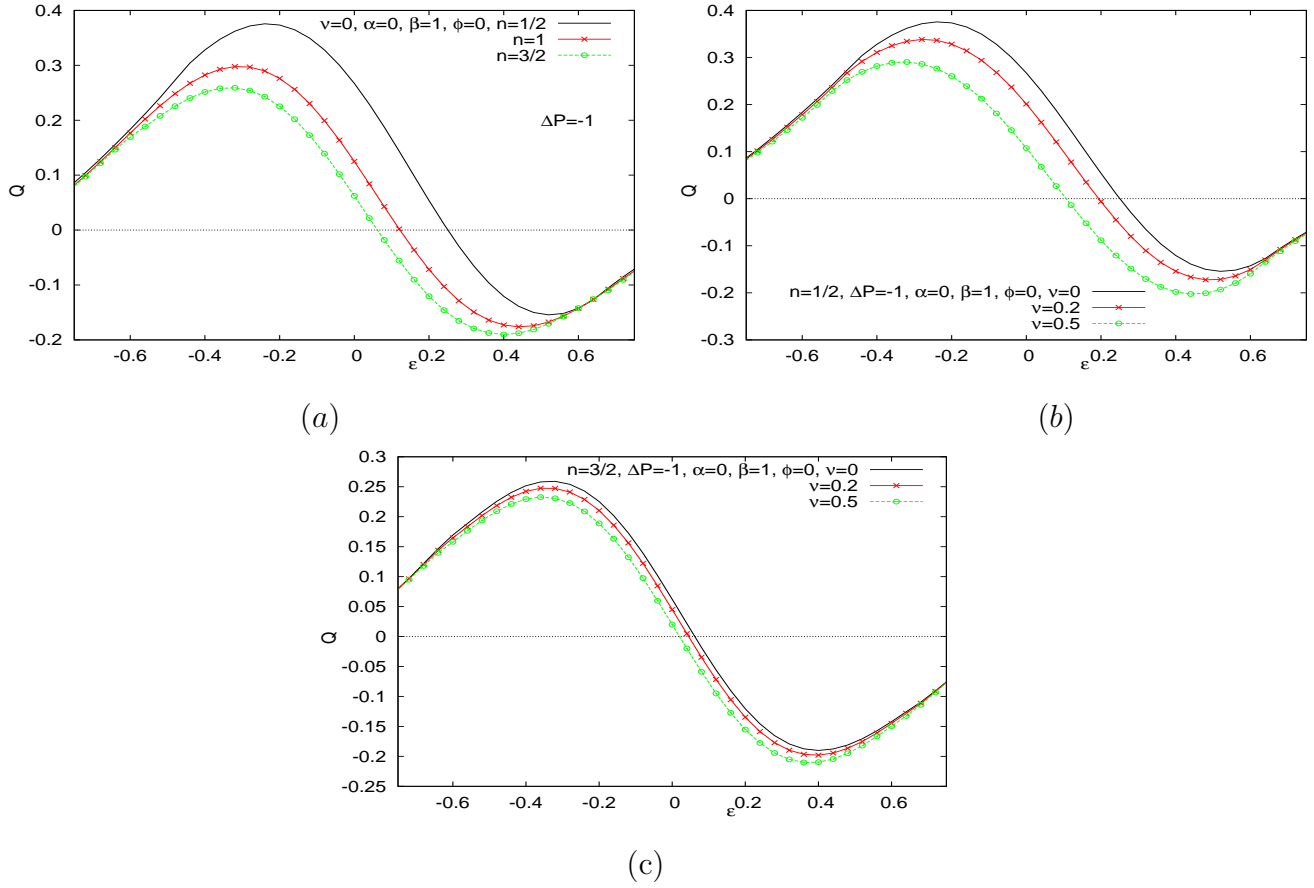


Figure 9: Variation of flow rate  $Q$  with the wall undulation amplitude  $\epsilon$  when  $k = 0$ ;  $\Delta P = -1$ ,  $\nu = 0$  to  $0.5$ ,  $\phi = 0$ ,  $\alpha = 0$ ,  $\beta = 1$  for a Newtonian fluid, shear-thinning fluid and shear-thickening fluid.

due to hydrodynamic forcing  $\Delta P$  only, electric forcing  $U_s$  only and combined action of  $\Delta P$  and  $U_s$  for Newtonian fluid ( $n = 1$ ), shear-thinning fluid ( $n = 1/2$ ) and shear-thickening fluid ( $n = 3/2$ ). Moreover, the linear sum of hydrodynamic forcing  $Q_{PO}$  and electric forcing  $Q_{EO}$  has been shown by the rectangular points. It is worthwhile to note the significant influence of the phase  $\phi$  on the distributions of  $Q_{PO}$ ,  $Q_{EO}$  and  $Q_{comb}$  for the flows in non-uniform vessels.  $Q_{EO}$  and  $Q_{comb}$  are enhanced gradually as the value of  $\phi$  increases in the interval  $0 < \phi < 1$  except in the limiting case of  $\phi = 1$ . It is important to note that the flow is taking place in the backward direction before  $\phi$  reaches a certain value (near 0.4) in the presence of an applied electric forcing. The sum of  $Q_{PO}$  and  $Q_{EO}$  is different from  $Q_{comb}$  at any phase shift for shear-thinning fluid and shear-thickening fluid (cf. Figs. 3-4). However, for Newtonian fluid (cf. Fig. 2),  $Q_{comb}$  is linear superposition of the hydrodynamic  $Q_{PO}$  and electrokinetic effects  $Q_{EO}$ . Thus for a non-Newtonian fluid, the linearity fails to hold when  $\epsilon$  and  $\beta$  are non-zero. It is interesting to note that  $Q_{PO} + Q_{EO} < Q_{comb}$  for shear-thinning fluid (cf. Fig. 3), but just opposite behaviour (i.e.  $Q_{PO} + Q_{EO} > Q_{comb}$ ) is observed for shear-thickening fluid (cf. Fig. 4). If either the radius of the tube or the wall charge distribution is non-uniform, pressure can be generated internally. In order to maintain the continuity of flow along the tube, this type of induced pressure is required. For a power-law fluid, it is well known that the flow rate varies non-linearly with the pressure gradient. However, for EOF, the pressure gradient is generated not only due to the hydrodynamic forcing, but also due to the electric forcing. As a result, the relationship between the flow rate and the two forcings is nonlinear for a non-Newtonian fluid flow in a tube of non-uniform cross section. However, the wall undulation can interact with the wall charge modulation differently for different values of the phase shift  $\phi$ . It is further to be noted that the flow rate is the maximum positive when  $\phi = \pi$  and is the negative and minimum when  $\phi = 0$ . The phases  $\phi = \pi$  and  $\phi = 0$  indicate the situations where the maximum positive/negative slip velocity arises at the narrowest section of the tube respectively. It also indicates that the electric forcing at the narrowest part of the tube has the most influence on the net flow. It further reveals the well known fact consistently, i.e., the flow rate is limited at the smallest cross-section of the channel/tube for the flow through a channel/tube with transverse topographical patterns. Given wall shape and HS slip modulation can interact with each other to give rise to the maximum positive effect on the flow when  $-\epsilon\beta \cos \phi$  is the maximum positive. Hence  $\phi = \pi$  if  $\epsilon\beta > 0$  and  $\phi = 0$  if  $\epsilon\beta < 0$ . It is worthwhile to mention that similar results are reported by Ng and Qi [110] for their study of EOF of a power-law fluid in a non-uniform micro-channel. However, the magnitude of the above results (i.e.  $Q_{PO}$ ,  $Q_{EO}$  and  $Q_{comb}$ ) for any

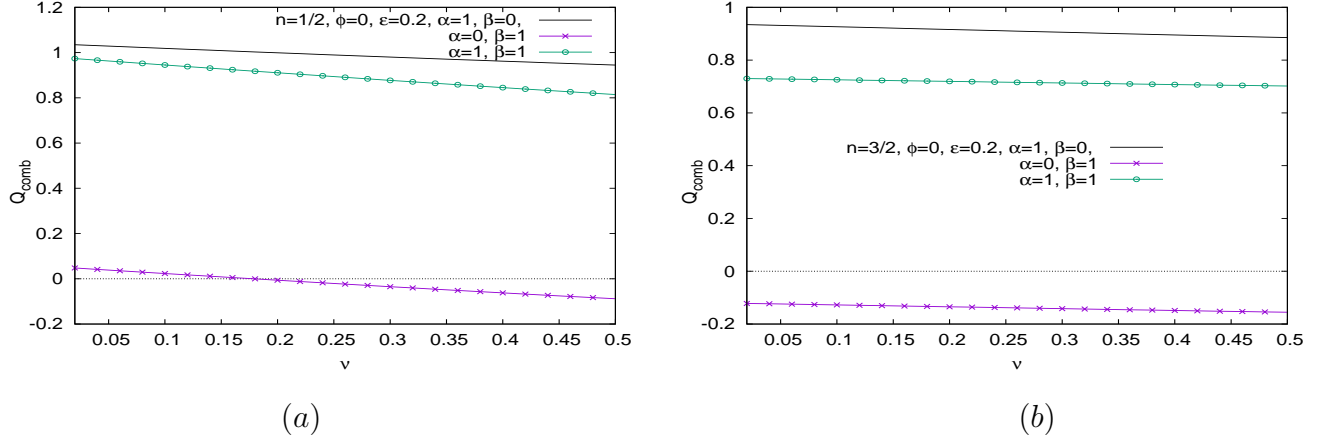


Figure 10: Variation of flow rate  $Q_{comb}$  with parameter  $\nu$  when  $k = 0$ ,  $\epsilon = 0.2$ ,  $\phi = 0$ ,  $\Delta P = -1$  (a) for a shear-thinning fluid ( $n = 1/2$ ), (b) for a shear-thickening fluid ( $n = 3/2$ ).

value of flow index number  $n$  have been reduced significantly (around half in magnitude) for EOF of a Herschel-Bulkley fluid in a tube of non-uniform cross section.

Variation of  $Q$  with respect to  $\phi$  is affected by the value of the parameter  $\nu$  only if an applied pressure force is active (cf. Figs. 3,4). The effect is prominent when both the electric and pressure force are acting (cf. Figs. 3(d),4(d)). The backward flow has been enhanced and the forward flow has been reduced with an increase in  $\nu$  due to resistance created by the yield stress. Moreover,  $\nu$  has relatively more influence on shear-thinning fluid than shear-thickening fluid.

Figs. 5 exhibit the variation of flow rate  $Q$  with the phase  $\phi$  for the cases due to  $Q_{PO}$ ,  $Q_{EO}$  and  $Q_{comb}$  in a tube with mean radius is of diverging/tapered nature. For the diverging case, the flow rate is gradually and significantly increasing with the increase of the inclination of the tube wall. Moreover, quantitative deviation of  $Q_{comb}$  from superimpose of  $Q_{PO}$  and  $Q_{EO}$  becomes more prominent. For the converging case, the reverse trend of  $Q$  has been observed compare to previous case, i.e.,  $Q$  is gradually decreasing at a similar percentage rate like the diverging case. However, when outlet tube radius is 25% of the inlet radius, then hydrodynamic force is negligible compare to the electrokinetic force and influence of  $\phi$  on  $Q$  is very less impactful. Moreover, volumetric flow ( $Q$ ) has been reduced significantly (near to zero) in this case. These results may be expected physically as the resistance to the flow decreases with the increases of free space in the tube for the diverging case. Whereas, for the converging case the resistance to the flow increases as the free space in the tube becomes narrower. Thus, converging/diverging nature of the mean tube radius plays vital role on the transport of a fluid.

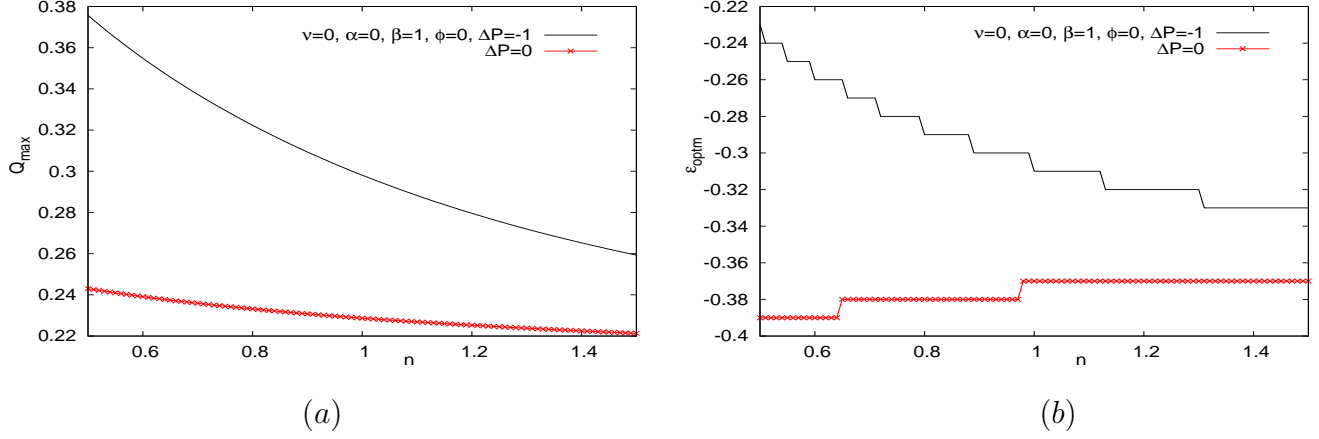


Figure 11: Variation of flow rate  $Q_{max}$  and corresponding  $\epsilon_{optm}$  with flow index number  $n$  for  $k = 0$ ,  $\nu = 0$ ,  $\phi = 0$ ,  $\alpha = 0$ ,  $\beta = 1$  (a) for  $Q_{max}$ , (b) for  $\epsilon_{optm}$ .

In Figs. 6, a different nature has been observed for a tube where the tube radius is of diverging/tapered nature (i.e.  $h = 1 + kZ$  and  $U_s = \alpha + \beta \cos(2\pi Z + \phi)$ ) when it is compared to Figs. 5. In this case,  $\phi$  is considered as the phase constant which can be interpreted using the initial amplitude at  $Z = 0$ . Up to a certain limit of  $\phi$ ,  $Q$  is decreasing with the increase of  $\phi$  in the diverging tube. If  $\phi$  crosses the limit, then  $Q$  is increasing with the increase of  $\phi$ . It is to be noted that the minimum values of  $Q_{comb}$  and the superimpose of  $Q_{PO}$  and  $Q_{EO}$  have not seen at the same limiting value of  $\phi$  as hydrodynamic force and electric force are not working linearly. We have found significant deviation of  $Q_{comb}$  from superimpose of  $Q_{PO}$  and  $Q_{EO}$  quantitatively for the case of a diverging tube. Since  $Q_{EO} < 0$  for all values of  $\phi$  except in the neighbourhood of 0, electric force is working in the backward direction. In the case of a converging tube,  $Q$  is increasing with the increase of  $\phi$  up to a certain limit of  $\phi$  and after then it is decreasing with the increase of  $\phi$ . However, the magnitudes of  $Q$  are found very less compare to the case of converging tube. It is due to the resistance created by a converging tube by reducing the area of tube.

The variation of flow rates with  $\epsilon$  for the cases  $Q_{PO}$ ,  $Q_{EO}$  and  $Q_{comb}$  of Newtonian and rheological fluids in uniformly charged walls ( $\alpha = 1$ ,  $\beta = 0$ ), which are without any phase (i.e.  $\phi = 0$ ), has been exhibited in Figs. 7. Also for this case, the sum of  $Q_{PO}$  and  $Q_{EO}$  is different from  $Q_{comb}$  for Non-Newtonian fluid except in the limiting case of  $\epsilon = 0$ . These figure also support our earlier statement that for any value of rheological parameter  $n$ , linearity works for a tube with uniform cross section (i.e.  $\epsilon = 0$ ,  $\beta = 0$ ). Here it is also further noticed that  $Q_{PO} + Q_{EO} < Q_{comb}$  for  $n < 1$  and  $Q_{PO} + Q_{EO} > Q_{comb}$  for  $n > 1$  (cf. Fig. 7). It has

been observed that when  $\beta = 0$ ,  $Q$  decreases monotonically with increasing  $\epsilon$  (cf. Figs. 7). For this case also, the magnitude of  $Q_{PO}$ ,  $Q_{EO}$  and  $Q_{comb}$  have been reduced appreciably to the corresponding case in micro-channel (cf. Ng and Qi [110]) although these behaviours are similar. Moreover, difference between  $Q_{comb}$  and  $Q_{PO} + Q_{EO}$  is clearly visible for a rheological fluid.

Like the previous case, variation of  $Q$  with respect to  $\epsilon$  is significantly affected by the value of the parameter  $\nu$  only if the pressure force is acting (cf. Figs. 7). The flow has been reduced clearly with an increase in  $\nu$  due to the resistance created by the yield stress.

Fig. 8 displays the distribution of flow rates of Newtonian and rheological fluids with the HS slip modulation amplitude  $\beta$  for  $\phi = 0$ ,  $\alpha = 1$  in a uniform tube. It reveals that the periodic variation of the HS slip has no net effect on the flow of a Newtonian fluid if the wall undulation is absent. This nature is irrespective of the pressure forcing.

The response to the pressure forcing is very different in the case of a shear-thinning and shear-thickening fluid. If the walls are flat and there is no applied pressure forcing (i.e.  $\Delta P = 0$ ), the flow rate is always unaffected by  $\beta$  for any  $n$  (cf. equation (29)). However, the contrary result is found in the presence of an applied pressure forcing (i.e.  $\Delta P \neq$  not equal to zero). In this case, it is seen that the flow rate for non-Newtonian fluid (i.e.  $n$  not equal to 1) significantly changed due to the change in  $\beta$ . For favorable pressure gradient (i.e.  $\Delta P < 0$ ), the flow rate  $Q$  increases with  $\beta$  for a shear-thinning fluid ( $n < 1$ ) and it decreases with  $\beta$  for a shear-thickening fluid ( $n > 1$ ). Fig. 8 further reveals that variation in the HS slip alone may interact non-linearly with the hydrodynamic forcing for a rheological fluid even in the absence of wall undulation (i.e.  $\epsilon = 0$ ).

Similar to the previous cases, variation of  $Q$  with respect to  $\beta$  is observed to reduce appreciably with an increase in  $\nu$  only if the pressure force is acting (cf. Fig. 8). However, the effect is more prominent here than the previous cases. Contrary to the Fig. 8,  $Q$  does not varying monotonically with increasing  $\epsilon$  when  $\beta$  not equal to zero (cf. Fig. 9). When  $\Delta P = -1$ ,  $\alpha = 0$ ,  $\beta = 1$ ,  $\phi = 0$ , Fig. 5 depicts how flow rate may vary non-monotonically with  $\epsilon$ . This behaviour appears due to the two competing effects.

It is observed that the area at the narrowest section decreases and hence the flow is reduced in this region when  $\epsilon$  increases in magnitude. However, on the other hand, since the interaction between the wall undulation and the slip modulation will become stronger, the flow will be augmented. At the narrowest section, as the radius of the tube tends to zero (i.e. at the limit  $\epsilon = \pm 1$ ), the flow rate  $Q$  will also tend to zero (Fig. 9). When  $\epsilon$  becomes zero, the correlation

term  $\epsilon\beta = 0$  and so the resulting flow rate  $Q$  is not the maximum. It is further observed that the maximum flow rate  $Q_{max}$  takes place at a negative value of  $\epsilon$ . As mentioned earlier, interaction of  $\epsilon$  and  $\beta$  will affect positively on  $Q$  if  $\epsilon\beta \cos \phi$  negative only. As exhibited in Fig. 9,  $Q$  becomes always positive for negative values of  $\epsilon$  and  $Q$  is always negative for positive values of  $\epsilon$ . Similar to the previous cases, it is seen that the variation of  $Q$  with respect to  $\epsilon$  is reduced significantly if we increase  $\nu$ .

Fig. 10 displays the distribution of flow rates  $Q_{comb}$  of a shear-thinning fluid ( $n = 1/2$ ) and shear-thickening fluid ( $n = 3/2$ ) with parameter  $\nu$  for  $k = 0$ ,  $\phi = 0$ ,  $\epsilon = 0.2$ . The flow has been observed to reduce with an increase in  $\nu$  (i.e. consequently related to yield stress) due to resistance created by the yield stress. Here, we can also note that the influence of yield stress and consequently  $\nu$  has relatively more effect on a shear-thinning fluid than a shear-thickening fluid.

Fig. 11 presents how the power-law index  $n$  makes influence on the maximum flow rate  $Q_{max}$  and the corresponding optimum undulation amplitude  $\epsilon_{optm}$ . It is observed that  $Q_{max}$  always decreases with increasing  $n$ .  $\epsilon_{optm}$  may rise or fall depending on  $\Delta P$ . It is being reduced in magnitude with increasing  $n$  if the hydrodynamic force is active. However,  $Q_{max}$  is seen to rise with an increase in  $n$  when hydrodynamic force is absent. Moreover, the change of  $\epsilon_{optm}$  for the case is not prominent to  $n$ . These behaviours again point out the nonlinear interaction between the hydrodynamic forcing and the electric forcing in driving the flow of a rheological fluid through a tube of non-uniform cross-section.

## 4 Summary and Conclusion

The present paper deals with a simplified study of the electrokinetic flow of a Herschel-Bulkley fluid. The flow is considered in a tube where the wall potential and tube radius is gradually varying along the axis of the tube. We have treated the slip condition, representing a thin Newtonian depletion layer enclosing a still thinner electric double layer, as Helmholtz–Smoluchowski (HS) slip type. The effects of the phase  $\phi$ , the wall undulation amplitude  $\epsilon$ , HS slip modulation amplitude  $\beta$ , the power-law index  $n$ , yield stress parameter  $\nu$  (the ratio between yield stress and wall shear stress) and the converging/diverging nature of the tube (i.e.  $k$ ) on the volumetric flow rate is investigated in different situations under the purview of the lubrication theory. The plots present a clear view of the qualitative and quantitative variation of various fluid mechanical parameters. It is observed that pressure can be generated internally under non-uniformity

in either the wall charge or in the cross section of the tube height, which will upset the linear relationship between flow and applied electric force for a non-Newtonian fluid. The wall undulation (i.e.  $\epsilon$ ) and the surface charge modulation (i.e.  $\beta$ ) may interact with each other when pressure and electric forces acting simultaneously. As a result, various nonlinear flow behaviors appear. The study reveals that the flow is a linear superimpose of the components due to the hydrodynamic and electric forcings for a Non-Newtonian bulk fluid only when the tube is of uniform cross section or when the flow is strictly one-dimensional. However, how much pressure can be generated internally and how the the hydrodynamic & electric forcings will interact each other that depend strongly on the rheology of the fluid (i.e. flow index number  $n$ ), wall undulation and boundary slip parameter. The effect of Newtonian depletion layer is to cause the flow rate to be insignificant for the power-law index  $n$  when the pressure force is inactive. Because if  $\Delta p = 0$  (i.e. there is no applied pressure forcing) and the tube radius is of uniform cross section, then the pressure gradient is insignificant globally as well as locally. Rheological fluid index  $n$  related to hydrodynamic force, i.e., related to variation of pressure/pressure gradient. Moreover, it is well known that the flow rate varies nonlinearly with the pressure gradient for a power-law fluid. Thus  $n$  has no significant influence on volumetric flow due to constant like pressure throughout the tube. As a result, a Non-Newtonian fluid acts Newtonian not only near the wall of the tube, but also throughout the tube.

In spite of the Newtonian depletion layer, the power-law rheology is appeared to be more influential on the flow in the presence of pressure force. The periodic change in HS slip is found no effect on the volumetric flow rate  $Q$  if the pressure force is inactive and  $\epsilon = 0$ . However, in the presence of pressure force, the periodic change of the wall potential has dissimilar effects on  $Q$  depending on  $n = 1$ ,  $n < 1$  and  $n > 1$ . This behaviour occurs even when the wall undulation is absent. In contrast, the effect of  $\nu$  on the volumetric flow rate  $Q$  is found prominent only when the pressure gradient is applied.

$Q$  is reducing gradually with increasing  $\epsilon$  when  $\beta = 0$ . However, there exists an optimum amplitude at which the flow rate is the maximum when  $\beta > 0$  and this maximum occurs where  $\epsilon_{optm}\beta \cos \phi < 0$ . The maximum flow rate and the corresponding optimum undulation amplitude may vary appreciably with the power-law index  $n$ .  $n$  makes strong influence on the maximum flow rate and the corresponding optimum undulation amplitude when the pressure force is present. It is important to mention that the converging/diverging nature of the tube radius plays a crucial role on the EOF of a rheological fluid.

There are many microfluidic processes involving various non-Newtonian Power-law fluids.

In order to dealing these fluids, the Smoluchowski velocity may be applied in order to predict the flow rates of the Power-law fluids in electrokinetically driven microfluidic devices. Since microstructures in electrokinetics-based microfluidic devices are complex, exact solutions are not available there. If we apply the slip velocity approach with the Smoluchowski velocity as the slip wall velocity, the numerical simulations may be simplified. However, there are the limitations for the applying of this assumption and also about the limitations on the validation of results as discussed in the introduction and formulation of the study.

**Acknowledgment:** *We thank the Reviewers and Associate Editor, Professor I. A. Frigaard for their useful comments, which helped to improve the paper. One of the authors, S. Maiti, is thankful to the University Grants Commission (UGC), New Delhi for awarding the Dr. D. S. Kothari Post Doctoral Fellowship during this investigation.*

## References

- [1] Li DQ (2004) Electrokinetics in Microfluidics. Elsevier, Amsterdam
- [2] Jacobson SC, Hergenröder R, Koutny LB, Warmack RJ, Ramsey JM (1994) Effects of Injection Schemes and Column Geometry on the Performance of Microchip Electrophoresis Devices. Anal Chem 66:1107-1113
- [3] Ermakov SV, Jacobson SC, Ramsey JM (2000) Computer Simulations of Electrokinetic Injection Techniques in Microfluidic Devices. Anal Chem 72:3512-3517
- [4] Hjerten S (1967) Free zone electrophoresis. Chromatographic Reviews 9:122
- [5] Chen HS, Chang HT (1999) Electrophoretic Separation of Small DNA Fragments in the Presence of Electroosmotic Flow Using Poly (ethylene oxide) Solutions. Anal Chem 71:2033-2036
- [6] Dutta P, Beskok A (2001) Analytical solution of combined electroosmotic/pressure driven flow in two dimensional straight channels: finite Debye Layer effects. Anal Chem 73:1979-1986
- [7] Reuss FF (1809) Charge Induced Flow. Proc Imp Soc Naturalists Moscou 3:327-344



- [8] Hunter RJ (1981) Zeta Potential in Colloid Science: Principle and Applications. Academic Press, London
- [9] Zhao CL, Yang C (2013) Electrokinetics of non-Newtonian fluids: a review. *Adv Colloid Interface Sci* 201:94-108
- [10] Wiedemann G (1852) First Quantative Study of Electrical Endomose. *Pogg Ann* 87:321
- [11] Helmholtz H (1879) Studien über electrische Grenzschichten. *Ann Phys* 243:337-382
- [12] Smoluchowski M (1903) Contribution à la théorie l'endosmose électrique et de quelques phénomènes corrélatifs. *Bull Int Acad Sci Cracovie* 8:182-199
- [13] Ermakov SV, Jacobson SC, Ramsey JM (1998) Computer simulations of electrokinetic transport in microfabricated channel structures. *Anal Chem* 70(21):4494-4504
- [14] Hunter RJ (1992) Foundations of colloid science, Vol I. Oxford University Press, Oxford
- [15] Hunter RJ (1992) Foundations of colloid science, Vol II. Oxford University Press, Oxford
- [16] MacInnes JM, Du X, Allen RWK (2003) Prediction of electrokinetic and pressure flow in microchannel T-junction. *Phys Fluids* 15:1992-2005
- [17] MacInnes JM (2002) Computation of reacting electrokinetic flow in micro-channel geometries. *Chem Eng Sci* 57:4539
- [18] Zimmerman WB, Rees JM, Craven TJ (2006) Rheometry of non-Newtonian electrokinetic flow in a microchannel T-junction. *Microfluid Nanofluidics* 2:481-492
- [19] Craven TJ, Rees JM, Zimmerman WB (2008) On slip velocity boundary conditions for electroosmotic flow near sharp corners. *Phys Fluids* 20:43603
- [20] Probstein RF (1994) Physicochemical Hydrodynamics, 2nd edition. Wiley, New York
- [21] Molho JM, Herr AE, Desphande M, Gilbert JR, Garguilo MG, Paul PH, John PM, Woudenberg TM, Connel C (1998). *Proc ASME (MEMS)* 66:69-76
- [22] Paul PH, Garguilo MG, Rakestraw DJ (1998) Imaging of Pressure and Electrokinetically Driven Flows through Open Capillaries. *Anal Chem* 70(13):2459-2467

- [23] Herr AE, Molho JI, Santiago JG, Mungal MG, Kenny TW, Garguilo MG (2000) Electroosmotic Capillary Flow with Nonuniform Zeta Potential. *Anal Chem* 72:1053-1057
- [24] Park HM, Lee WM (2008). Helmholtz-Smoluchowski velocity for viscoelastic electroosmotic flows. *J Colloid Interface Sci* 317:631-636
- [25] Xuan X, Li D (2005) Electroosmotic flow in microchannels with arbitrary geometry and arbitrary distribution of wall charge. *J Colloid Interface Sci* 289:291-303
- [26] Patankar NA, Hu HH (1998) Numerical simulation of electroosmotic flow. *Anal Chem* 70:1870
- [27] Mitchell MJ, Qiao R, Aluru NR (2000) Meshless analysis of steady state electro-osmotic transport. *J Microelectromech Syst* 9:435
- [28] Ghosal Sb (2002) Lubrication theory for electro-osmotic flow in a microfluidic channel of slowly varying cross-section and wall charge. *J Fluid Mech* 459:103-128
- [29] Sinton D, Xuan C, Li D (2004) Thermally induced velocity gradients in electroosmotic microchannel flows: The cooling influence of optical infrastructure. *Exp Fluid* 37:872-882
- [30] Xuan X, Li D (2005) Band broadening in capillary zone electrophoresis with axial temperature gradients. *Electrophoresis* 26: 166-175
- [31] Bianchi F, Ferrigno R, Girault HH (2000) Finite Element Simulation of an Electroosmotic Driven Flow Division at a t-Junction of Microscale Dimensions. *Anal Chem* 72:1987-1993
- [32] Erickson D, Li D (2002) Influence of Surface Heterogeneity on Electrokinetically Driven Microfluidic Mixing. *Langmuir* 18:1883-1892
- [33] Ajdari A (2000) Pumping liquids using asymmetric electrode arrays. *Phys Rev E* 61:R45-R48
- [34] Oddy MH, Santiago JG, Mikkelsen JC (2001) Electrokinetic Instability Micromixing. *Anal Chem* 73:5822-5832
- [35] Dutta P, Beskok A (2001) Analytical Solution of Time Periodic Electroosmotic Flows: Analogies to Stokes' Second Problem, *Anal Chem* 73:5097-5102

- [36] Rubin S, Tulchinsky A, Gat AD, Bercovici M (2017) Elastic deformations driven by non-uniform lubrication flows. *J Fluid Mech* 812:841-865
- [37] Vinogradova OI (1999) Slippage of water over hydrophobic surfaces. *Intl J Miner Process* 56(1):31-60
- [38] Baudry J, Charlaix E, Tonck A, Mazuyer D (2001) Experimental evidence for a large slip effect at a nonwetting fluid–solid interface. *Langmuir* 17(17):5232-5236
- [39] Yariv E (2004) Electro-osmotic flow near a surface charge discontinuity. *J Fluid Mech* 521:181-189
- [40] Khair AS, Squires TM (2008) Surprising consequences of ion conservation in electro-osmosis over a surface charge discontinuity. *J Fluid Mech* 615:323-334
- [41] Iadecola C, Yang G, Ebner T, Chen G (1997) Local and propagated vascular responses evoked by focal synaptic activity in cerebellar cortex. *Neurophysiol* 78:651-659
- [42] Pulgar VM (2015) Direct electric stimulation to increase cerebrovascular function. *Front Syst Neurosci* 9:54
- [43] Lang N, Siebner HR, Ward NS, Lee L, Nitsche MA, Paulus W, et al. (2005) How does transcranial DC stimulation of the primary motor cortex alter regional neuronal activity in the human brain? *Eur J Neurosci* 22:495-504
- [44] Nonnekes J, Arrogi A, Munneke MAM, van Asseldonk EHF, Oude Nijhuis LB, Geurts AC, et al. (2014) Subcortical structures in humans can be facilitated by transcranial direct current stimulation. *PLoS ONE* 9:e107731
- [45] Thakral G, Lafontaine J, Najafi B, et al. (2013) Electrical stimulation to accelerate wound healing. *Diabet Foot Ankle* 4:22081
- [46] Velmahos GC, Petrone P, Chan LS, Hanks SE, Brown CV, Demetriades D (2005) Electrostimulation for the prevention of deep venous thrombosis in patients with major trauma: a prospective randomized study. *Surgery* 137:493-498
- [47] Doran FS, Drury M, Sivyer A (1964) A simple way to combat the venous stasis which occurs in the lower limbs during surgical operations. *Br J Surg* 51:486-492

- [48] Doran FS, White HM (1967) A demonstration that the risk of postoperative deep venous thrombosis is reduced by stimulating the calf muscles electrically during the operation. *Br J Surg* 54:686-689
- [49] Doran FS, White M, Drury M (1970) A clinical trial designed to test the relative value of two simple methods of reducing the risk of venous stasis in the lower limbs during surgical operations, the danger of thrombosis, and a subsequent pulmonary embolus, with a survey of the problem. *Br J Surg* 57:20-30
- [50] Rajendran SB, Challen K, Wright KL, Hardy JG (2021) Electrical Stimulation to Enhance Wound Healing. *J Funct Biomater* 12:40
- [51] Ud-Din S, Bayat A (2014) Electrical Stimulation and Cutaneous Wound Healing: A Review of Clinical Evidence. *Healthcare* 2:445-467
- [52] Hampton S, Collins F (2006) Treating a pressure ulcer with bio-electric stimulation therapy. *Br J Nurs* 15:S14-S18
- [53] Arora M, Harvey LA, Glinsky JV, Nier L, Lavrencic L, Kifley A, Cameron ID (2020) Electrical stimulation for treating pressure ulcers. *Cochrane Database Syst Rev* 1:Cd012196
- [54] Kloth LC (2014) Electrical Stimulation Technologies for Wound Healing. *Adv Wound Care* 3:81-90
- [55] Watanabe H, Takahashi H, Nakao M, Walton K, Llinás RR (2009) Intravascular neural interface with nanowire electrode. *Electro Commun Japan* 92:29-37
- [56] Clover AJ, McCarthy MJ, Hodgkinson K, Bell PR, Brindle NP (2003) Noninvasive augmentation of microvessel number in patients with peripheral vascular disease. *J Vasc Surg* 38:1309-1312
- [57] Allen NJ, Barres BA (2009) Neuroscience: Glia – more than just brain glue. *Nature* 457(7230):675-677
- [58] Tsytsarev V, Hu S, Yao J, Maslov K, Barbour DL, Wang LV (2011) Photoacoustic microscopy of microvascular responses to cortical electrical stimulation. *J Biomed Opt* 16

- [59] Tsytsarev V, Premachandra K, Takeshita D, Bahar S (2008) Imaging cortical electrical stimulation in vivo: fast intrinsic optical signal versus voltage-sensitive dyes. *Opt Lett* 33(9):1032-1034
- [60] Zonta M, Angulo MC, Gobbo S, Rosengarten B, Hossmann KA, Pozzan T, Carmignoto G (2003) Neuron-to-astrocyte signaling is central to the dynamic control of brain microcirculation. *Nat Neurosci* 6(1):43-50
- [61] Choi YS, Hsueh YY, Koo J, et al. (2020) Stretchable, dynamic covalent polymers for soft, long-lived bioresorbable electronic stimulators designed to facilitate neuromuscular regeneration. *Nat Commun* 11:5990
- [62] Jones S, Man WD, Gao W, et al. (2016) Neuromuscular electrical stimulation for muscle weakness in adults with advanced disease. *Cochrane Database Syst Rev* 10: CD009419
- [63] Hong Z, Sui M, Zhuang Z, Liu H, Zheng X, Cai C, Jin D (2018) Effectiveness of neuromuscular electrical stimulation on lower limbs of patients with hemiplegia after chronic stroke: a systematic review. *Arch Phys Med Rehabil* 99:1011-1022.e1
- [64] Willand MP, Rosa E, Michalski B, Zhang JJ, Gordon T, Fahnstock M, Borschel GH (2016) Electrical muscle stimulation elevates intramuscular BDNF and GDNF mRNA following peripheral nerve injury and repair in rats. *Neuroscience* 334:93-104
- [65] Loaiza LA, Yamaguchi S, Ito M, Ohshima N (2002) Vasodilatation of muscle microvessels induced by somatic afferent stimulation is mediated by calcitonin gene-related peptide release in the rat. *Neurosci Lett* 333(2):136-40
- [66] Tan JS, Lin CC, Chen GS (2020) Vasomodulation of peripheral blood flow by focused ultrasound potentiates improvement of diabetic neuropathy. *BMJ Open Diabetes Res Care* 8:e001004
- [67] Berli CLA, Olivares ML (2008) Electrokinetic flow of non-Newtonian fluids in microchannels. *J Colloid Interface Sci* 320:582-589
- [68] Berli CLA (2010) Output pressure and efficiency of electrokinetic pumping of non-Newtonian fluids. *Microfluidics and Nanofluidics* 8:197-207

- [69] Bandopadhyay A, Chakraborty S (2011) Steric-effect induced alterations in streaming potential and energy transfer efficiency of non-Newtonian fluids in narrow confinements. *Langmuir* 27:12243-12252
- [70] Misra JC, Maiti S (2012) Peristaltic transport of rheological fluid: model for movement of food bolus through esophagus. *Appl Math Mech* 33(3):15-32
- [71] Misra JC, Maiti S (2012) Peristaltic pumping of blood through small vessels of varying cross-section. *J Appl Mech, ASME* 22(8):061003
- [72] Maiti S, Misra JC (2013) Non-Newtonian characteristics of peristaltic flow of blood in micro-vessels. *Commun Nonlinear Sci Numer Simul* 18:1970-1988
- [73] Maiti S, Misra JC (2012) Peristaltic Transport of a Couple Stress Fluid: Some Applications to Hemodynamics. *J Mech Medi Biol* 12(3):1250048
- [74] Barnes HA (1995) A review of the slip (wall depletion) of polymer solutions, emulsions and particle suspensions in viscometers: its cause, character, and cure. *J Non-Newtonian Fluid Mech* 56:221-251
- [75] Tuinier R, Taniguchi T (2005) Polymer depletion-induced slip near an interface. *J Phys: Condensed Matter* 17:L9-L14
- [76] Olivares ML, Vera-Candiotti L, Berli, CLA (2009) The EOF of polymer solutions. *Electrophoresis* 30:921-929
- [77] Das S, Chakraborty S (2006) Analytical solutions for velocity, temperature and concentration distribution in electroosmotic microchannel flows of a non-Newtonian bio-fluid. *Anal Chimica Acta* 559:15-24
- [78] Merrill EW (1969) Rheology of blood. *Physiol Reviews* 49:863
- [79] Nguyen QD, Boger DV (1983) Yield stress measurement for concentrated suspensions. *J Rheol* 27:321
- [80] Bird RB, Dai GC, Yarusso BJ (1983) The rheology and flow of viscoplastic materials. *Rev Chem Eng* 1:1
- [81] Frigaard I (2019) Simple yield stress fluids, *Curr. Opin Coll Sci* 22:638-663

- [82] Balmforth N, Frigaard IA, Ovarlez G (2014) Yielding to stress: recent developments in viscoplastic fluid mechanics. *Annu Rev Fluid Mech* 46:121146
- [83] Coussot P (2014) Yield stress fluid flows: a review of experimental data. *J Non-Newtonian Fluid Mech* 211:31-49
- [84] Bonn D, Denn M, Berthier B, Divoux B, Manneville S (2017) Yield stress materials in soft condensed matter. *Rev Mod Phys* 89:035005.
- [85] Huilgol RR (2015) *Fluid mechanics of viscoplasticity*, Springer
- [86] Ovarlez G, Hormozi S (2019) *Lectures on visco-plastic fluid mechanics*, Springer
- [87] Cloitre M, Bonnecaze RT (2017) A review on wall slip in high solid dispersions. *Rheol Acta* 56:283-305
- [88] Coussot P (2017) Bingham's heritage. *Rheol Acta* 56:163-176
- [89] Ewoldt R, McKinley G (2017) Mapping thixo-elasto-visco-plastic behavior. *Rheol Acta* 56:195-210
- [90] Frigaard I, Paso G, de Souza Mendes PR (2017) Bingham's model in the oil and gas industry. *Rheol Acta* 56:259-282
- [91] Malkin A, Kulichikhin V, Ilyin S (2017) A modern look on yield stress fluids. *Rheol Acta* 56:177-188
- [92] Mitsoulis E, Tsamopoulos J (2017) Numerical simulations of complex yield-stress fluid flows. *Rheol Acta* 56:231-258
- [93] Saramito P, Wachs A (2017) Progress in numerical simulation of yield stress fluid flows. *Rheol Acta* 56:211-230
- [94] de Souza Mendes P, Thompson R (2019) Time-dependent yield stress materials. *Curr Opin Colloid Interface Sci* 43:15-25.
- [95] Fusi L (2018) Channel flow of viscoplastic fluids with pressure-dependent rheological parameters. *Phys Fluids* 30:073102

- [96] Putz A, Frigaard IA, Martinez DM (2009) On the lubrication paradox and the use of regularization methods for lubrication flows. *J Non-Newtonian Fluid Mech* 163:62-77
- [97] Lipscomb G, Denn M (1984) Flow of Bingham fluids in complex geometries. *J Non-Newtonian Fluid Mech* 14:337-346
- [98] Frigaard IA, Ryan DP (2004) Flow of a visco-plastic fluid in a channel of slowly varying width. *J Non-Newtonian Fluid Mech* 123:67-83 .
- [99] Muravleva L (2015) Squeeze plane flow of viscoplastic Bingham material. *J Non-Newtonian Fluid Mech* 220:148-161
- [100] Wilson S (1993) Squeezing flow of a Bingham material. *J Non-Newtonian Fluid Mech* 47:211-219
- [101] Muravleva L (2018) Squeeze flow of Bingham plastic with stick-slip at the wall. *Phys Fluids* 30:030709
- [102] Fusi L, Farina A (2003) An extension of the Bingham model to the case of an elastic core. *Adv Math Sci Appl* 13(1):113-163 .
- [103] Fusi L, Farina A and Rosso F (2012) Flow of a Bingham-like fluid in a finite channel of varying width: A two-scale approach. *J Non-Newtonian Fluid Mech* 177:76-88
- [104] Fusi L, Farina A, Rosso F, Roscani S (2015) Pressure-driven lubrication flow of a Bingham fluid in a channel: A novel approach. *J Non-Newtonian Fluid Mech* 221:66-75
- [105] Fusi L, Farina A, Rosso F (2016) Squeeze flow of a Bingham-type fluid with elastic core. *Int J Nonlinear Mech* 78:59-65
- [106] Walton IC, Bittleston SH (1991) The axial flow of a Bingham plastic in a narrow eccentric annulus. *J Fluid Mech* 222:39-60
- [107] Pinkus O, Sternlicht B (1961) *Theory of Hydrodynamic Lubrication*. McGraw-Hill, New York
- [108] Liu Y, Liu Y, Guo Q, Yang J (2009) Modeling of electroosmotic pumping of nonconducting liquids and biofluids by a two-phase flow method. *J Electro Chem* 636:86



- [109] Tang GH, Ye PX, Tao WQ (2010) Pressure-driven and electroosmotic non-Newtonian flows through microporous media via lattice Boltzmann method. *J Non-Newtonian Fluid Mech* 165:1536
- [110] Ng CO (2013) Combined pressure-driven and electroosmotic flow of Casson fluid through a slit microchannel. *J Non-Newtonian Fluid Mech* 198:1
- [111] Bharti RP, Harvie DJE, and Davidson MR (2009) Electroviscous effects in steady fully developed flow of a power-law liquid through a cylindrical microchannel. *Inter J Heat and Fluid Flow* 30:804
- [112] Zhao C, Yang C (2010) Nonlinear Smoluchowski velocity for electroosmosis of power-law fluids over a surface with arbitrary zeta potentials. *Electrophoresis* 31:973
- [113] Zhao C, Yang C (2011) Electro-osmotic mobility of non-Newtonian fluids. *Biomicrofluidics* 5:014110
- [114] Vasu N, De S (2010) Electroosmotic flow of power-law fluids at high zeta potentials. *Colloids Surf: A Physicochem Eng Asp* 368:44
- [115] Babaie A, Sadeghi A, Saidi MH (2011) Combined electroosmotically and pressure driven flow of power-law fluids in a slit microchannel. *J Non-Newtonian Fluid Mech* 166:792
- [116] Vakili MA, Sadeghi A, Saidi MH, Mozafari AA (2012) Electrokinetically driven fluidic transport of power-law fluids in rectangular microchannels. *Colloids Surf: A Physicochem Eng Asp* 414:440
- [117] Chakraborty S (2007) Electroosmotically driven capillary transport of typical non-Newtonian biofluids in rectangular microchannels. *Anal Chimica Acta* 605:175-184
- [118] Zhao C, Zholkovskij E, Masliyah J, Yang C (2008) Analysis of electroosmotic flow of power-law fluids in a slit microchannel. *J Colloid Inter Sci* 326:503-510
- [119] Tang GH, Li XF, He YL, Tao, WQ (2009) Electroosmotic flow of non-Newtonian fluid in microchannels. *J Non-Newtonian Fluid Mech* 157:133-137
- [120] Zhao C, Yang C (2009) Analysis of power-law fluid flow in a microchannel with electrokinetic effects. *Inter J Emerg Multidisci Fluid Sci* 1:37-52

- [121] Zhao C and Yang C (2013) Electroosmotic flows of non-Newtonian power-law fluids in a cylindrical microchannel. *Electrophoresis* 34:662-667
- [122] Ng CO, Qi C (2013) Electroosmotic flow of a viscoplastic material through a slit channel with walls of arbitrary zeta potential. *Phys Fluids* 25:103102
- [123] Herschel WH, Bulkley R (1926) Konsistenzmessungen von Gummi-Benzollosungen. *Kolloid Zeitschrift* 39:291-300
- [124] Scott-Blair GW, Spanner DC (1974) *An Introduction to Biorheology*. Elsevier Scientific Publishing Company, Amsterdam
- [125] Das B (1991) Entrance region flow of the Hershel-Bulkley fluid in a circular tube. *Fluid Dyn Res* 10:39-53
- [126] Nallapu S, Radhakrishnamacharya G (2016) A Two-Fluid Model for Herschel-Bulkley Fluid Flow through Narrow Tubes. *J Appl Sci Eng* 19(3):241-248
- [127] Moreno E, Larese A, Cervera M (2016) Modelling of Bingham and Herschel–Bulkley flows with mixed P1/P1 finite elements stabilized with orthogonal subgrid scale. *J Non-Newtonian Fluid Mech* 228:1-16
- [128] Iida N (1978) Influence of Plasma Layer on Steady Blood Flow in Microvessels. *Jap J Appl Phys* 17(1):203
- [129] Vajravelu K, Sreenadh S, Devaki P, Prasad K (2011) Mathematical model for a Herschel-Bulkley fluid flow in an elastic tube. *Centr Eur J Phys* 9(5):1357-1365
- [130] Minatti L, Pasculli A (2011) SPH numerical approach in modelling 2D muddy debris flow, in: *International Conference on Debris-Flow Hazards Mitigation: Mechanics, Prediction, and Assessment*:467–475
- [131] Remaitre A, Malet JP, Maquaire O, Ancy C, Locat J (2005) Flow behaviour and runout modelling of a complex debris flow in a clay-shale basin. *Earth Surf Process Landf* 30(4):479-88
- [132] Ajdari A (1996) Generation of transverse fluid currents and forces by an electric field: electro-osmosis on charge-modulated and undulated surfaces. *Physical Review E* 53:4996-5005

- [133] Ajdari A (2001) Transverse electrokinetic and microfluidic effects in micropatterned channels: lubrication analysis for slab geometries. *Physical Review E* 65:016301
- [134] Long D, Stone HA, Ajdari A (1999) Electroosmotic flows created by surface defects in capillary electrophoresis. *J Colloid Interface Sci* 212:338-349
- [135] Ng CO, Zhou Q (2012) Electro-osmotic flow through a thin channel with gradually varying wall potential and hydrodynamic slippage. *Fluid Dyn Res* 44:055507
- [136] Ng CO, Zhou Q (2012) Dispersion due to electroosmotic flow in a circular microchannel with slowly varying wall potential and hydrodynamic slippage. *Phys Fluids* 24:112002
- [137] Ng CO, Qi C (2014) Electroosmotic flow of a power-law fluid in a non-uniform microchannel. *J Non-Newtonian Fluid Mech* 208-209:118-125
- [138] Dey P, Shit GC (2020) Electroosmotic flow of a fractional second-grade fluid with interfacial slip and heat transfer in the microchannel when exposed to a magnetic field. *Heat Transfer* 50(3):2643-2666
- [139] Ranjit NK, Shit GC (2019) Entropy generation on electromagnetohydrodynamic flow through a porous asymmetric micro-channel. *Euro J Mech/B Fluids* 77:135-147
- [140] Ranjit NK, Shit, GC, Tripathi D (2019) Entropy generation and Joule heating of two layered electroosmotic flow in the peristaltically induced micro-channel. *Inter J Mech Sci* 153-155:430-444
- [141] Mondal A, Shit GC (2018) Electro-osmotic flow and heat transfer in a slowly varying asymmetric micro-channel with Joule heating effects. *Fluid Dyn Research* 50:065502
- [142] Ranjit NK, Shit GC, Tripathi D (2018) Joule heating and zeta potential effects on peristaltic blood flow through porous micro vessels altered by electrohydrodynamic. *Microvas Research* 117:74-89
- [143] Ranjit NK, Shit GC (2017) Joule heating effects on electromagnetohydrodynamic flow through a peristaltically induced micro-channel with different zeta potential and wall slip. *Physica A: Statis Mech appl* 482:458-476

- [144] Khan AI, Dutta P (2019) Analytical Solution of Time-Periodic Electroosmotic Flow through Cylindrical Microchannel with Non-Uniform Surface Potential. *Micromachines* 10:498
- [145] Lee JSH, Ren CL, Li D (2005) Effects of surface heterogeneity on flow circulation in electroosmotic flow in microchannels. *Anal Chimica Acta* 530:273-282
- [146] Kim H, Khan AI, Dutta P (2019) Time-Periodic Electro-Osmotic Flow With Nonuniform Surface Charges. *ASME J Fluids Eng* 141(8):081201
- [147] Green NG, Ramos A, Gonzalez A, Morgan H, Castellanos A (2000) Fluid Flow Induced by Nonuniform AC Electric Fields in Electrolytes on Microelectrodes. I. Experimental Measurements, *Physical Review E* 61(4):4011-4018
- [148] Potoček B, Gaš B, Kenndler E, Štědrý M (1995) Electroosmosis in Capillary Zone Electrophoresis with Non-uniform Zeta Potential. *J Chromatogr A*, 709(1):51-62
- [149] Horiuchi K, Dutta P, Ivory CF (2007) Electroosmosis with Step Changes in Zeta Potential in Microchannels. *AIChE Journal* 53(10):2521-2533
- [150] Chang CC, Yang RJ (2006) A Particle Tracking Method for Analyzing Chaotic Electroosmotic Flow Mixing in 3D Microchannels with Patterned Charged Surfaces. *J Micromech Microeng* 16(8):1453-1462
- [151] Green NG, Ramos A, Gonzalez A, Morgan H, Castellanos A (2002) Fluid flow induced by nonuniform ac electric fields in electrolytes on microelectrodes. III. Observation of streamlines and numerical simulation. *Phys Rev E* 66:026305